Research Square

Preprints are preliminary reports that have not undergone peer review.
They should not be considered conclusive, used to inform clinical practice,
or referenced by the media as validated information.

Solanum torvum Leaf-Mediated Phytogenic Engineering of Zn- and Sr-Doped MgO Nanoparticles as an Efficient Photocatalyst

M Sivaperumal

msiva.chemistry@gmail.com

Knowledge Institute of Technology (Autonomous)

G Raja

Paavai Engineering College (Autonomous)

S Surendhiran

Karpagam College of Engineering

N Kandhasamy

Sengunthar Engineering College

Research Article

Keywords: Solanum torvum, green synthesis, MgO nanoparticles, Zn-MgO, Sr-MgO, Methylene Blue, Photocatalytic degradation

Posted Date: September 4th, 2026

DOI: https://doi.org/10.21203/rs.3.rs-10794448/v1

License: This work is licensed under a Creative Commons Attribution 4.0 International License.
Read Full License

Additional Declarations: No competing interests reported.

Solanum torvum Leaf-Mediated Phytogenic Engineering of Zn- and Sr-Doped MgO Nanoparticles as an Efficient Photocatalyst

Sivaperumal M[1, *], Raja G[2], Surendhiran S[3,4], Kandhasamy N[5]

[1]Department of Chemistry, Knowledge Institute of Technology (Autonomous)
Kakapalayam, Salem – 637 504, Tamil Nadu, India

[2]Department of Chemistry, Paavai Engineering College (Autonomous)
Pachal, Namakkal – 637 018, Tamil Nadu, India

[3]Department of Science and Humanities, Karpagam College of Engineering
Coimbatore – 641 032, Tamil Nadu, India

[4]Centre for Energy and Environment, Karpagam Academy of Higher Education
Coimbatore – 641 021, Tamil Nadu, India

[5]Department of Chemistry, Sengunthar Engineering College (Autonomous)
Tiruchengode, Namakkal – 637 205, Tamil Nadu, India

Abstract

The development of sustainable semiconductor photocatalysts through green synthetic strategies has emerged as an effective approach for environmental remediation. In this study, Zn- and Sr-doped MgO nanoparticles were successfully synthesized via a facile phytogenic route using *Solanum torvum* leaf extract as a natural reducing and stabilizing agent. The structural, morphological, optical, and chemical properties of the synthesized nanoparticles were systematically investigated using X-ray diffraction (XRD), Fourier transform infrared spectroscopy (FT-IR), UV–visible diffuse reflectance spectroscopy (UV-DRS), SEM-EDX, high-resolution transmission electron microscopy (HR-TEM), selected area electron diffraction (SAED), and X-ray photoelectron spectroscopy (XPS). XRD analysis confirmed the formation of phase-pure face-centered cubic MgO without secondary impurity phases, with average crystallite sizes of 15.6, 11.2, and 12.85 nm for pure MgO, Zn-doped MgO, and Sr-doped MgO, respectively. FT-IR spectra exhibited the characteristic Mg-O stretching vibration at 598 cm^{-1}, confirming oxide formation. UV-DRS analysis revealed significant bandgap narrowing from 3.59 eV for pristine MgO to 2.31 eV and 2.57 eV for Zn- and Sr-doped MgO, respectively, demonstrating enhanced visible-light absorption resulting from dopant-induced electronic structure modulation. SEM-EDX, HR-TEM, SAED, and XPS analyses verified the successful incorporation of Zn and Sr into the MgO lattice while revealing highly crystalline nanoparticles with uniform morphology and appropriate elemental

composition. The photocatalytic performance was evaluated through the degradation of methylene blue under different pH values, catalyst dosages, and dye concentrations. Among the synthesized catalysts, Zn-doped MgO exhibited the highest photocatalytic efficiency under optimized conditions, followed by Sr-doped MgO and pristine MgO. The superior photocatalytic activity is attributed to the synergistic effects of crystallite size reduction, enhanced visible-light harvesting, dopant-induced bandgap narrowing, and suppressed electron-hole recombination, which collectively promote the generation of reactive oxygen species responsible for dye mineralization. This study demonstrates that *Solanum torvum*-mediated Zn-doped MgO nanoparticles represent an environmentally benign and highly efficient photocatalyst with significant potential for sustainable wastewater treatment and advanced environmental remediation.

Keywords: *Solanum torvum*, green synthesis, MgO nanoparticles, Zn-MgO, Sr-MgO, Methylene Blue, Photocatalytic degradation

1. Introduction

Water contamination has emerged as one of the most challenging global environmental concerns, driven by rapid industrialization and urbanization, as well as unregulated effluent discharges. The industrial sectors include textiles, pharmaceuticals, cosmetics, paper, medical, and food (Nadimi et al. 2018; Tang et al. 2022). These industries discharge significant volumes of untreated industrial effluents containing organic dyes, heavy metals, surfactants, solvents, pesticides, and other xenobiotics into aquatic ecosystems (Panchal et al. 2021),(Taghavi Fardood et al. 2023). Among these environmental contaminants, synthetic dyes, such as methylene blue (MB), a heterocyclic cationic dye widely used in textile dyeing, constitute a particularly hazardous class because of their chemical stability, aromatic structures, and resistance to natural biodegradation. These industrially sourced synthetic dyes persist in aquatic environments, significantly altering photosynthetic activity and disrupting aquatic food webs (Paul et al.). Furthermore, chronic exposure to dye-contaminated water has been associated with respiratory disorders, dermatological complications, and systemic toxicity (mutagenicity, carcinogenicity, and endocrine disruption) in humans and animals (Aldawsari et al. 2021; Hassan et al. 2022; Hotan Alsohaimi et al. 2023). Hence, the adoption of an efficient and eco-friendly strategy to address this global concern is urgently required.

Various physicochemical and biological approaches, such as adsorption, coagulation–flocculation, reverse osmosis, electrochemical oxidation, activated sludge processes, membrane filtration, and advanced oxidation treatments, have been explored to manage MB contamination (Fouda et al. 2021; Lin et al. 2022; Kandasamy et al. 2026). However, these approaches have limitations, including the production of secondary contaminants, high operational costs and energy consumption, incomplete mineralization, and membrane fouling (Kuruthukulangara and Asharani 2024). Therefore, there is growing interest among environmental scientists in developing sustainable, cost-effective, and environmentally benign remediation technologies capable of achieving complete dye degradation rather than merely

phase transfer. In these circumstances, metal oxide nanoparticle-mediated photocatalysis has gained substantial attention as a green and energy-efficient approach for the mineralization of MB. Metal oxide nanoparticles have emerged as promising photocatalysts for wastewater remediation applications owing to their nanoscale dimensions, high surface-to-volume ratios, tunable bandgap energies, and superior redox properties (Chayed et al. 2019).

Metal oxide nanoparticles such as TiO_2, ZnO, MgO, Fe_3O_4, CuO, SnO_2, CeO_2, $CoFe_2O_4$, WO_3, and ZrO_2 have emerged as photocatalysts for degrading organic pollutants(Kalam et al. 2018; Ruíz-Baltazar et al. 2019; Li et al. 2019; Ayvacikli et al. 2020; Shimi et al. 2022a; Vinayagam et al. 2022; Saadabadi et al. 2024) Among these metal oxide nanomaterials, MgO nanoparticles have been widely used in photocatalysis, medicine, sensors, water treatment, anticancer and antimicrobial applications, and agriculture (Naren Vidaarth et al. 2024). These applications have attracted increasing interest because of their low toxicity, low band gap, high thermal stability, chemical inertness, and cost-effectiveness (Muhaymin et al. 2024). However, pristine MgO possesses a relatively wide bandgap, which restricts visible-light absorption and limits its photocatalytic efficiency. To overcome this limitation, metal-ion doping has been widely adopted as a strategy for engineering electronic band structures. Dopant incorporation can induce lattice distortion, generate oxygen vacancies, narrow the bandgap, and improve charge carrier separation, collectively enhancing the photocatalytic performance (Shkir et al. 2024b).

Although several studies have reported single-metal doping in MgO systems, co-doping strategies remain underexplored, particularly those involving synergistic combinations of alkaline earth and transition metals (TMs). The simultaneous incorporation of Zn (Zn^{2+}) and Sr (Sr^{2+}) ions is expected to induce complementary electronic and structural modifications within the MgO lattice. Zn doping can effectively narrow the bandgap and enhance optical absorption, whereas Sr incorporation can introduce lattice strain and defect states that promote charge separation and the generation of reactive radicals. Despite this theoretical potential, integrated

Zn- and Sr-doped MgO nanostructures for photocatalytic dye remediation have not been systematically investigated to date.

Numerous methods have been developed for synthesizing MgO NPs, including hydrothermal, sol-gel, solvothermal, co-precipitation, laser ablation, green synthesis, and spray pyrolysis methods(Gong et al. 2016; Wang et al. 2021; Namakka et al. 2023; Srinivasan and Rana 2024). These traditional preparation techniques have several limitations, including the use of toxic substances, excessive heat requirements, and the generation of byproducts that can be hazardous to the environment; the removal of by-products and toxic pollutants from wastewater using traditional nanomaterial synthesis methods remains the greatest challenge. To overcome these difficulties, plant extract-mediated synthesis of metal oxide nanoparticles has attracted substantial attention in recent years, owing to its environmentally friendly, low-cost, and non-toxic nature (Shahzadi et al. 2025; Endla 2025). Among medicinal plants, *Solanum torvum* (Turkey berry) is a metabolite-rich yet underutilized bioresource that contains glycoalkaloids, flavonoids, tannins, saponins, vitamins, and iron complexes, which can act as reducing agents and chelating agents, and also stabilize the formation of metal oxide nanoparticles (Muhaymin et al. 2024). Hence, the present study was designed to synthesize Zn- and Sr-doped MgO nanoparticles, characterize them using various analytical techniques, and evaluate their photocatalytic degradation efficiency for methylene blue (MB).

2. Experiments and methodology

2.1 Materials and chemicals

High-purity chemicals such as magnesium nitrate hexahydrate ($Mg(NO_3)_2.6H_2O$), strontium nitrate hexahydrate ($Sr(NO_3)_2.6H_2O$), and zinc nitrate hexahydrate ($Zn(NO_3)_2.6H_2O$) were purchased from Nice Chemicals Pvt. Ltd. Methylene blue was obtained from Merck & Co. *S. torvum* leaves were collected from local farmers in Salem, Tamil Nadu, India

2.2 Preparation of *S. torvum* leaf extract:

The collected *S. torvum* leaves were cut into small pieces and washed with distilled water. The samples were further washed with double-distilled water (DD H_2O) to remove impurities, such as dust particles and other materials. For extraction, 100 ml of DD water was added to the finely cut leaves and boiled in a water bath at 70 °C for 60 min. The dark brown extract was obtained, cooled to room temperature, and filtered through Whatman No. 1 filter paper.

2.3 Green Synthesis of MgO and Zn-doped MgO nanoparticles

Plant extract (50 ml) was transferred into a 100 ml beaker and heated at 60°C using a magnetic stirrer. Approximately 2.5 g of $Mg(NO_3)_2 \cdot 6H_2O$ was dissolved in 15 ml of DD water, and 150 mg of Zn $(NO_3)_2.6H_2O$ was dissolved in 5 ml of DD water. $Mg(NO_3)_2 \cdot 6H_2O$ solution was added dropwise to the plant extract under vigorous stirring on a magnetic stirrer. After 10 min, a $Zn(NO_3)_2 \cdot 6H_2O$ solution was added dropwise to the plant extract and boiled at 60 °C. The mixture was then transferred into a silica crucible and dried at 180 °C for 4 h. After drying, the samples were washed several times with DD water to remove impurities. The samples were washed with ethanol three times to remove unreacted compounds and then dried at 120°C for 1 h. The dried samples were then annealed at 600°C for 6 h in a muffle furnace, and Zn-MgO nanoparticles were formed, as shown in Fig. 1.

2.4 Green Synthesis of Sr-doped MgO nanoparticles

Approximately 2.38 g of $Mg(NO_3)_2 \cdot 6H_2O$ was dissolved in 15 mL of DDH_2O, and 120 mg of Sr (NO3)2·6H2O was dissolved in 5 mL of DDH_2O. The $Mg(NO_3)_2 \cdot 6H_2O$ solution was added slowly to a freshly prepared 50 ml plant extract under constant stirring on a magnetic stirrer and boiled at 60°C. $Sr(NO_3)_2 \cdot 6H_2O$ was then added drop by drop under vigorous stirring with a magnetic stirrer. The solution mixture was then transferred to a crucible and dried at 180°C for 3 h. After drying, the powder samples were washed thrice with ethanol to remove impurities and dried at 120°C for 1 h. Subsequently, the powdered mixture was annealed in a muffle furnace at 600 °C for 6 h, yielding Sr-doped MgO nanoparticles, as shown in Fig. 1.

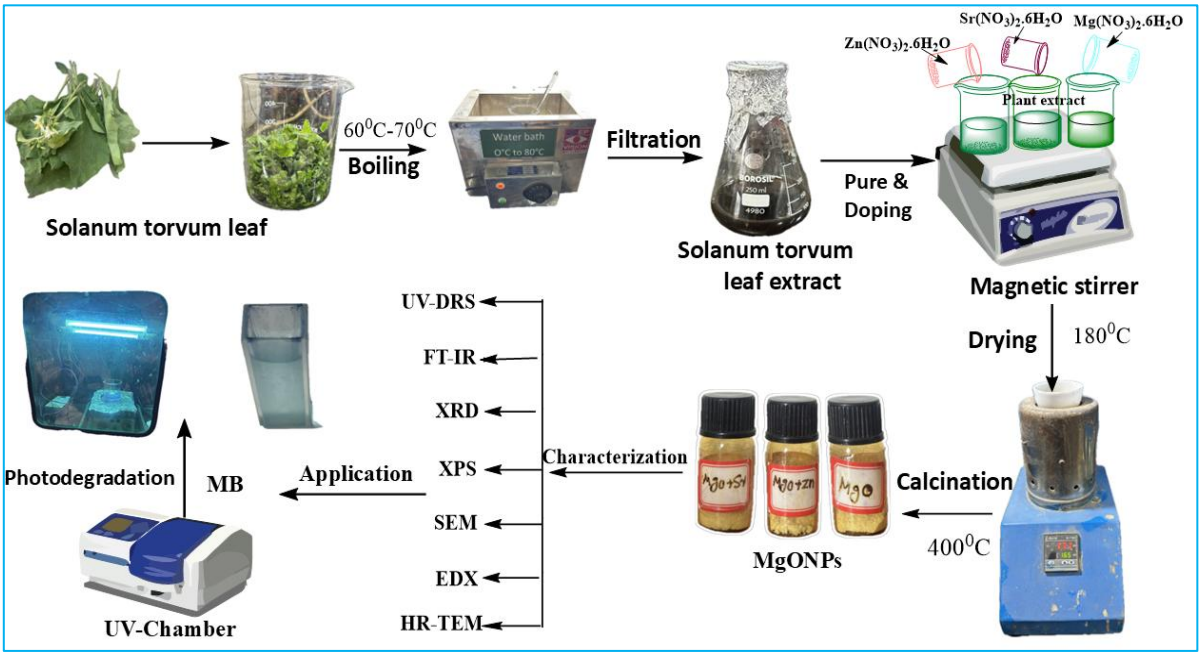


Fig.1. Schematic diagram of green synthesis of pure MgO, Zn-doped and Sr-doped MgO NPS by *S. torvum* leaf extract

2.5 Photo-catalytic degradation activity

The photocatalytic efficiency of green-synthesized Zn-doped and Sr-doped MgO NPs was investigated in the present study for methylene blue dye degradation at various catalytic and dye concentrations under a UV light source with a 40 W deuterium lamp. Different catalytic doses of 5, 15, 35, and 50 mg of Zn- and Sr-doped MgO NPs were combined with 10, 20, 35, and 50 ppm of MB solution, respectively, and allowed to stir for 45 min in the dark to attain adsorption-desorption equilibrium by achieving uniform dispersion. Subsequently, 4 ml of the solution was centrifuged at 12,000 rpm and exposed to UV light. The UV-Vis spectrophotometer wavelength of 663 nm was used to measure the absorption of solutions at various time intervals of 15 min each, followed by 90 min. The photocatalytic efficiency for dye degradation was calculated by applying the following formula (1)

$$\text{Degradation Efficiency (\%)} = \frac{C_0 - C_t}{C_0} \times 100 \quad (1)$$

In this formula, C_0 indicates the absorbance at the initial time, and C_t represents the absorbance at time t

2.6 Characterization techniques

The green-synthesized pure MgO, Zn-doped MgO, and Sr-doped MgO nanoparticles were confirmed by various instrumental analyses, including X-ray diffraction (XRD), Fourier transform infrared spectroscopy (FT-IR), UV-diffuse reflectance spectroscopy (DRS), X-ray photoelectron spectroscopy (XPS), high-resolution transmission electron microscopy (HRTEM-SAED), scanning electron microscopy (SEM), and energy-dispersive X-ray spectroscopy (EDAX). XRD analysis using Cu-Kα radiation with a wavelength of 1.5406 Å and 2θ = 10°–80° was used to examine the structural properties of the synthesized pure and doped MgO NPs. The chemical environment, elemental state, and binding energy of the pure, Zn-, and Sr-doped MgO NPs were investigated using XPS analysis (PHI 5000 VERSAPROBE III, Physical Electronics). FT-IR spectroscopy in the wavelength range of 400–4000 cm^{-1} was used to identify the presence of various functional groups in the green-synthesized NPs. The bandgap energy and optical properties of the synthesized NPs were investigated using UV-DRS. The crystalline structure, size, and shape of the green-synthesized Zn and Sr-doped MgO were confirmed by HR-TEM and SAED investigations. The structural morphology and elemental composition of the NPs were analyzed using SEM and EDX.

3. Results and discussion

3.1 Structural Analysis

The crystal nature and structural features of the green-synthesized photocatalysts were examined using an XRD diffractometer. The sample was then pressed into the sample holder, and the diffraction pattern (2θ= 20-80^0) was recorded. The diffraction patterns of ZS-doped MgO are presented in Fig. 2. The noticeable 2θ peaks observed at 36.84,42.96,62.36, and 74.7,78.6 are associated with crystal planes (111), (200), (220), (311), and (222), respectively, and the observed peaks are well matched with JCPDS No. (87—0653), and the peaks represent the cubic structure (face-centered cubic (fcc)) of the pure MgO and ZS-MgO nanoparticles [30], [31]. This spectrum implies that while Zn and Sr were doped into the MgO lattice, no significant distortions were observed. No other peaks associated with ZnO or SrO were

observed. The green-synthesized Zn- and Sr-doped MgO NPs exhibited sharp and intense XRD peaks at approximately 42.9 (200), indicating the high crystallinity of pure and doped MgO NPs. The various structural parameters, such as average crystalline size (D), interplanar spacing (d) of pure and doped MgO NPs, were calculated by using Scherrer's equation (eq.2) and Bragg's equation (eq.3) (Singh et al. 2021; Yousefi et al. 2021)

$$D = \frac{0.9\lambda}{\beta \cos\theta} \quad (2)$$

$$n\lambda = 2d\sin\theta \quad (3)$$

where 'λ' is the wavelength of Cu-kα radiation (0.1542 nm), 'β' is the full-width-half-maximum (FWHM) in radians, 'd' is the interplanar distance, and 'θ' is the Bragg's angle of diffraction (radians). Furthermore, the lattice constant α_0, specific surface area (SA) of pure and Zn, Sr-doped MgO NPs were determined by employing the equation (eq.4,5) (D'Souza et al. 2021; Singh et al. 2021)

$$a_0 = d_{hkl} = \sqrt{h^2 + k^2 + l^2} \quad (4)$$

$$SA = \frac{6\times10^3}{D\times\rho} \quad (5)$$

where α_0 is the lattice constant $\alpha_{0=(}$a=b=c), '*hkl*'is the Miller scale value, 'D' is the average crystalline size, and ρ is the density of pure MgO (3.59g/cm^2). In addition to that, dislocation density (δ) and Lattice strain (ε) were measured via formulas (6,7).(Muhaymin et al. 2024)

$$\delta = \frac{n}{D^2} \quad (6)$$

$$\varepsilon = \frac{\beta cos\theta}{4} \quad (7)$$

The calculated structural parameters were obtained using the aforementioned formulas and are listed in Table 1. The average crystalline size of ZS-doped MgO was 15. 6nm (MgO), 11.2 nm (Zn-MgO), and 12. 8nm (Sr-MgO. This indicates the insertion of Zn and Sr into the MgO crystal lattice and the elevation of oxygen vacancy defects, which act as new nucleation sites for the configuration of new crystallites and reduce the crystal size. Identical results have

been observed (Rajendran et al. 2018; Almontasser and Parveen 2022). The surface areas of doped MgO (Zn-MgO: 148.9 nm^2 and Sr-MgO: 130.6 nm^2) were comparatively larger than that of MgO (107.2 nm^2) nanoparticles, indicating that doping increases the available surface area (Shkir et al. 2024a).

The lattice constant 'α_0' of MgO was measured to be 0.422nm, which shows an exceptional 'rock salt structure of MgO (Hornak 2021). However, a small difference in the lattice constant was noted, considering the different ionic sizes of Mg^{2+} ions and the dopants. Several studies have reported lattice differences. D'Souza et al (D'Souza et al. 2021) reported a borderline increase in the lattice constant $'\alpha_0'$ from 4.2189Å to 4.2201Å for MgO and Zn doped MgO, which the doping approach generates homogeneous strain, based on them which the doping approach generates homogeneous strain, based on them. These results may enhance the photocatalytic efficiency of MgO NPs.

Table 1. Structural parameters of green-synthesized pure MgO, Zn-doped MgO, and Sr-doped MgO NPs from the crystal plane (200) value

NPs	**2θ (^{0})**	**FWHM (β)**	**Average Crystalline Size (D)**	**Interplanar distance spacing d(nm)**	**Lattice constant, α_0 (nm)**	**Specific surface area (SA)(m^2/g)**	**Dislocation density (δ) (nm^{-2})**	**Lattice strain (ε)**
MgO - Pure	42.8	0.572	15.6	2.11	0.422	107.2	0.002	0.009
Zn-MgO	42.7	0.794	11.2	2.12	0.424	148.9	0.007	0.013
Sr-MgO	44.9	0.696	12.85	2.10	0.421	130.6	0.006	0.012

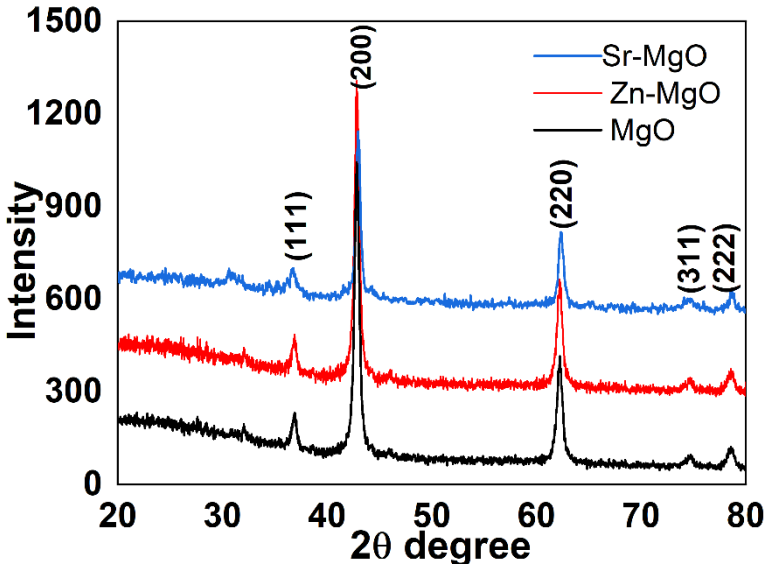


Fig. 2. XRD pattern of pure MgO, Zn and Sr-doped MgO NPs using *S.torvum* leaf extract

3.2 UV-DRS Analysis:

The optical properties of nanomaterials play a significant role in their photocatalytic activity. In UV spectroscopy, electrons are excited from a lower energy level (ground state) to a higher energy level (excited state) by absorbing the energy of a photon. The green-synthesized MgO, Zn, and Sr-doped MgO NPs were analyzed through UV-DRS spectra in the range from 200-800nm and are shown in Fig.3(a-c). The formation of MgO nanoparticles was confirmed by the absorption peak at 275 nm (Patil et al. 2024). The Zn-MgO nanoparticles exhibited an intense peak at 378 nm, which represented a red shift upon doping towards a longer wavelength due to the incorporation of Zn^{2+} ions into the Mg^{2+} ion lattice surface and a narrowing of the band gap (Vasanthi et al. 2017). The peak of Sr-doped MgO nanoparticles at 289 nm is attributed to a slight red shift. The absorption towards longer wavelengths (lower energy) red-shifted, while the doping of Zn and Sr in MgO NPs represented the introduction of defects. The optical band-gap energies of pure MgO, Zn-doped MgO, and Sr-doped MgO nanoparticles were estimated from the Kubelka–Munk plots and were found to be 3.59, 2.31, and 2.57 eV, respectively. (Eq. (8) (Makuła et al. 2018) and provide the obtained data in Table 2.

$$(F_{(r)}\ hv)^2 = B(hv - Eg) \qquad (8)$$

Where $F_{(r)}$ represents the Kubelka-Munk function, B is a constant, in which h is Planck's constant, v is the energy of the photon, and Eg represents the bandgap of the synthesized nanomaterials.

Table 2. UV-DRS and bandgap for Zn- and Sr- doped MgO NPs

Parameters	Nanoparticles		
	MgO	Zn-doped MgO	Sr-doped MgO
λmax (nm)	275 nm	378 nm	289 nm
Band gap Eg(eV)	3.59 eV	2.31 eV	2.57 eV

The bandgap of the synthesized nanomaterials enhances their optical and electronic properties. Fig.3(d-f) illustrates the bandgap (Eg) values of MgO, Zn-MgO, and Sr-MgO nanoparticles. The bandgap (Eg) value of MgO was found to be 3.59 eV, which is lower than that of bulk MgO (7.8 eV). The substantial reduction in band-gap energy after Zn and Sr incorporation confirms the successful modification of the electronic structure of MgO. (Hornak 2021). Among the synthesized materials, Zn-doped MgO exhibited the lowest band-gap value, indicating enhanced visible-light absorption capability. The narrowing of the band gap can be attributed to the introduction of defect states and lattice distortions arising from the substitution of Mg^{2+} ions by Zn^{2+} and Sr^{2+} ions within the MgO crystal lattice(Saleh et al. 2016; Zwijnenburg 2021). While doping with metal ions such as Zn and Sr, which alter the bandgap, is observed due to the addition of Zn^{2+} ions (0.74 Å) into the Mg^{2+} lattice sites (0.72 Å), it causes lattice distortions owing to the size mismatch. These distortions influence the electronic band structure and narrow the band gap energy by modifying the crystal field (Mohan et al. 2024). The bandgap of Sr-doped MgO nanoparticles is 2.57 eV, which is lower than that of MgO nanoparticles (3.59 eV). The bandgap difference is observed because of the larger ionic radius of Sr^{2+} (1.18 Å) compared to that of Mg^{2+}(0.72 Å), which alters the MgO crystal structure by introducing lattice strain and distortion. This structural change reduces the bandgap (Eg) energy

by reducing the band edge position. These structural and electronic modifications facilitate charge-carrier generation and migration, thereby enhancing the photocatalytic activity of the doped MgO nanoparticles. Consequently, the reduced band-gap energies of Zn-MgO and Sr-MgO nanoparticles contribute to their superior photocatalytic performance compared with pure MgO.

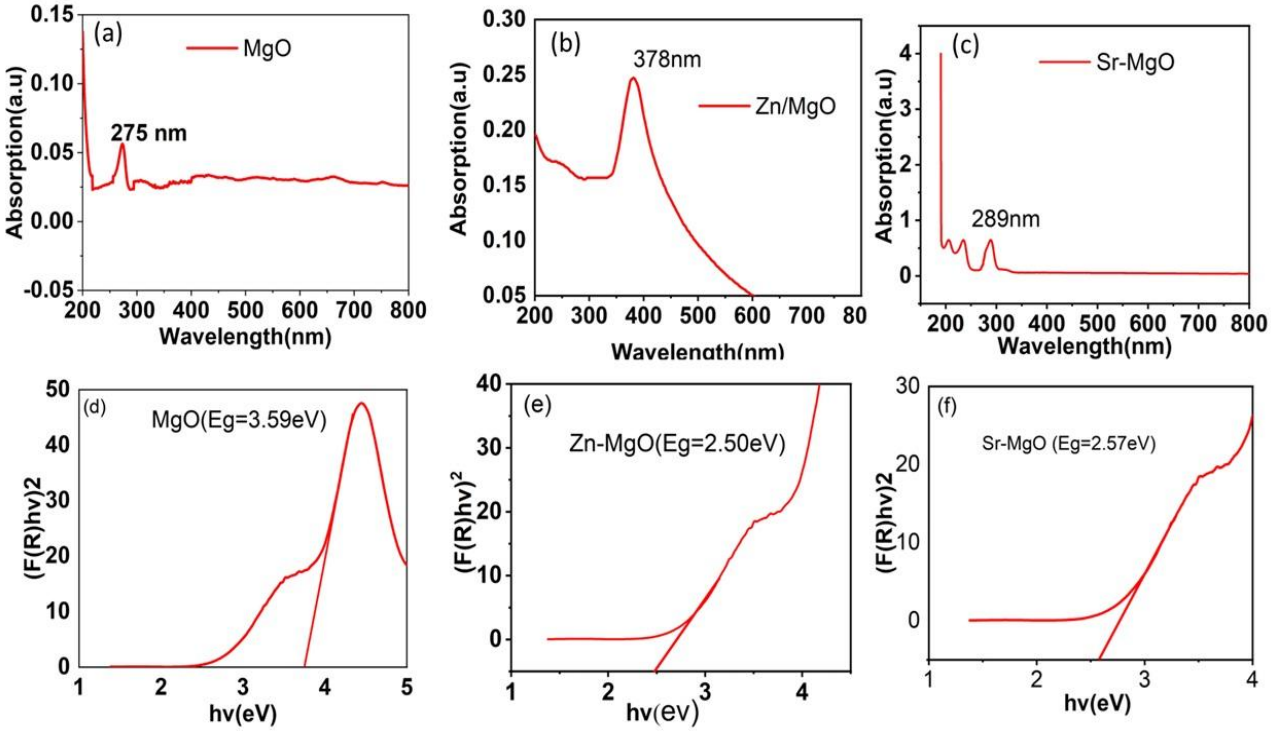


Fig.3. (a-c) UV-DRS (a) MgO (b) Zn-MgO (c) Sr-MgO, (d-f) Bandgap (d) MgO(e) Zn-MgO and (f) Sr-MgO

3.3 FT-IR Spectroscopy

The FT-IR spectra of the synthesized pure MgO, Zn-doped MgO, and Sr-doped MgO NPs using *Solanum torvum* leaf extract are shown in Fig. 4b. FT-IR spectroscopy was used to determine the various functional groups present in the synthesized MgO and Zn- and Sr-doped MgO NPs in the range of 4000- 400 cm^{-1}. A broad and prominent absorption band was observed at 3419 cm ^{1}, 3448 cm^{-1}, and 3428 cm^{-1}, which indicated the presence of O-H stretching vibrations of hydroxyl groups (Chauhan et al. 2024). The absorption bands at 2927 cm^{-1}, 2852 cm ^{1}, 2928 cm^{-1}, and 2923 cm^{-1} correspond to the symmetric and asymmetric C-H vibrations of methyl (CH_3) and methylene (CH_2) groups (Kuruthukulangara and Asharani 2023). A medium-sharp

absorption peak was observed at 1642 cm −1, and 1641 is attributed to the carbonyl group (C=O) stretching vibration of the amide group(Benisha et al. 2022). Additionally, the absorption peaks observed at 1423 cm ¹, 1407 cm^{-1}, and 1450 cm^{-1} correspond to the C-H bending of alkane, O-H groups containing carboxylic acids, and alcohols, respectively (Vinayagam et al. 2022). However, the peaks observed at 1113, 1053, and 1039 cm^{-1} are attributed to the CO stretching modes of alcohols and anhydrides. The low-frequency peaks observed at 615 cm^{-1} and 598 cm^{-1} are attributed to the metal oxide stretching vibrations, which represent the formation of metal oxide NPs, such as MgO and Zn/Sr-doped MgO NPs (Ramanujam and Sundrarajan 2014). The primary functional groups present in this leaf are saponins, flavonoids, glycosides, tannins, and alkaloids (Shah et al. 2021). At present, the existence of these functional groups in *S. torvum* extract is involved as the capping agent in the reduction process of metal ions (Pugazhendhi and Jayavel 2023).

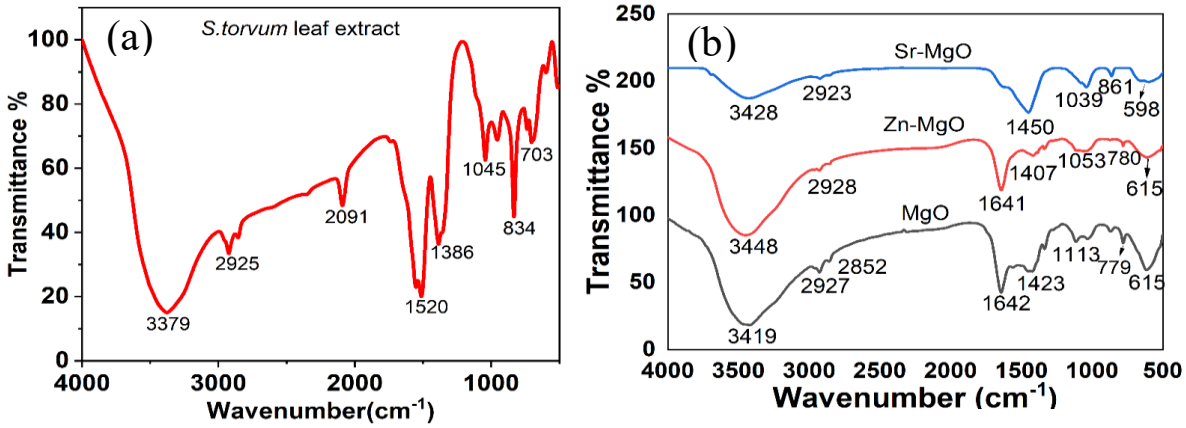


Fig.4. FT-IR analysis of *S.torvum* leaf extract (a) and Zn and Sr-doped MgO NPs (b)

3.4 Morphology studies

Fig.5(a-f) illustrates SEM and EDX spectra for the green-synthesized MgO photocatalysts, which give information about surface morphology and elemental composition. The SEM images show that the presence of voids and loosely crowded particles formed a sponge-like structure with an irregular shape and small agglomerations. The presence of porosity in the particles and an uneven, rough surface might improve the surface area.

Fig. 5(d-f) reveals the elemental composition of the MgO, Zn, and Sr-doped MgO nanoparticles. The EDX spectrum in Fig.5 d. confirms the presence of Mg and O in MgO, and Fig.5 (e, f) shows the doping of Zn and Sr in MgO nanoparticles. The high characteristic peaks of Mg and low-intensity peaks of Zn and Sr in the EDX spectrum confirm the doping of Zn and Sr at low concentrations on the surface of MgO nanoparticles. No additional peaks were observed, indicating the purity of the nanoparticles.

The structural morphology and SAED pattern of green-synthesized MgO, Zn, and Sr-doped MgO NPS were examined using high-resolution transmission electron microscopy (HRTEM), as shown in Fig. 6(a-c). HRTEM images provide valuable information about the crystalline size, shape, and crystal planes of the pure and doped MgO nanoparticles. The HRTEM images revealed that the MgO and doped nanoparticles show spherical particles with slight agglomeration, with an average particle size of 14 nm for pure MgO,11 nm for Zn-MgO, and 12.6 nm for Sr-doped MgO nanoparticles. The obtained average particle size matched the average crystalline size derived from the XRD findings. The SAED patterns showed bright spots along with concentric rings, representing the polycrystalline nature of pure MgO, Zn-doped MgO, and Sr-doped MgO NPs, which are attributed to the Miller scale values of 111, 200, 220, 311, and 222 of planes of the MgO lattice (Chauhan et al. 2024). The observed results clearly correlate with the XRD analysis.

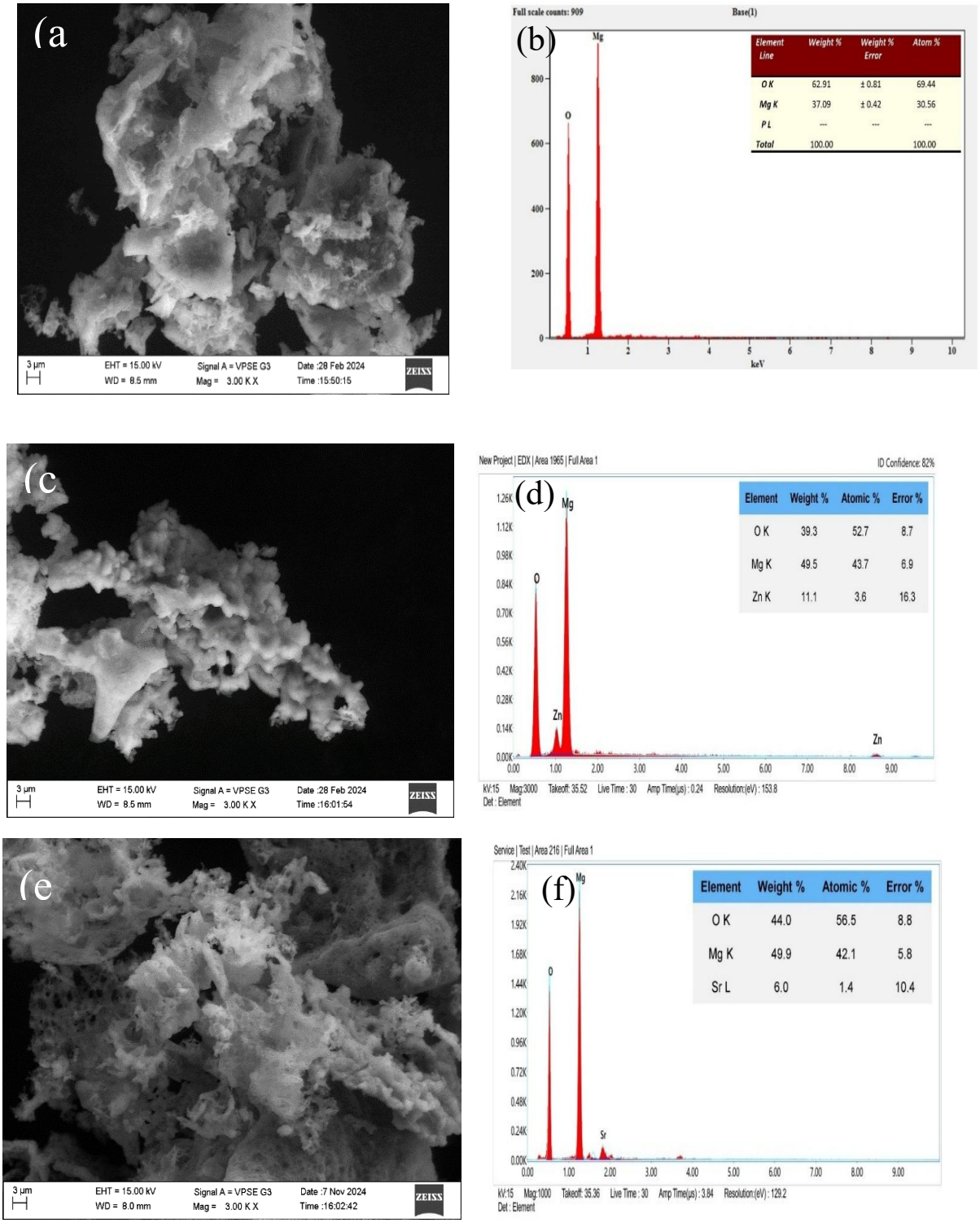


Fig.5. Morphology studies SEM with EDX (a & b) MgO, (c & d) Zn-MgO, and (e & f) Sr-MgO

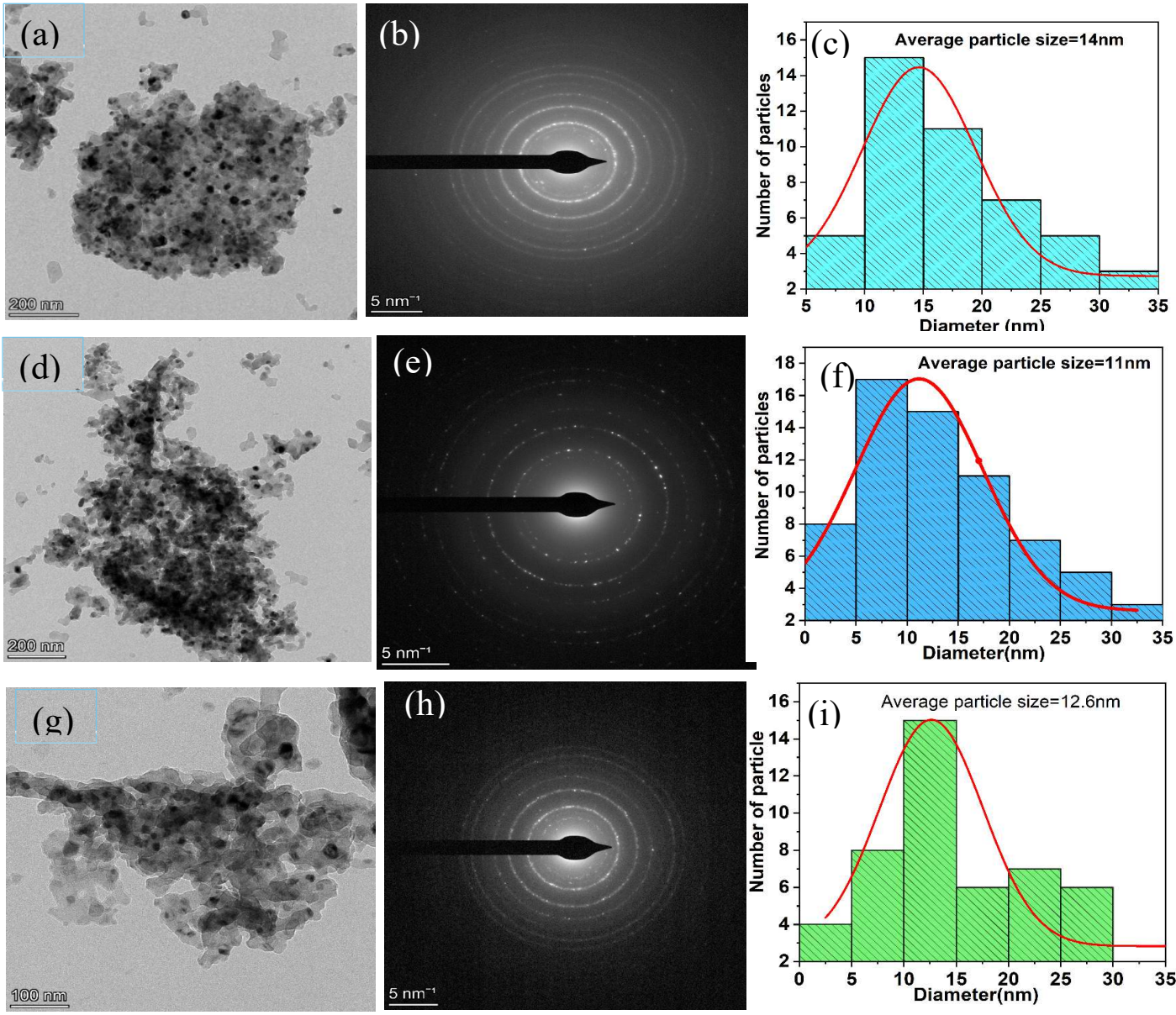


Fig.6.Morphology studies HRTEM, SAED, and average particle size of (a-c) MgO, (d-f) Zn-MgO, and (g-i) Sr-MgO nanoparticles.

3.5 XPS studies

X-ray photoelectron spectroscopy (XPS) was employed to investigate the elemental composition, chemical states, and surface electronic environment of the synthesized nanoparticles, which are critical factors influencing photocatalytic activity. Fig.7(a-e) illustrates the survey scan (a), deconvolution spectrum of Mg 1s (b), deep scan O1s spectrum (c), deep scan Zn 2p spectrum (d), and Sr 3d spectrum (e) of ZS-doped MgO nanoparticles. The O1S peak observed at 531.6 eV for MgO, 531.5eV for Zn-MgO, and 531.4 eV for Sr-MgO is attributed to the lattice oxygen and surface oxygen species, as represented in Fig.7 c. These

oxygen-containing surface sites can act as active centres for generating reactive oxygen species (ROS), such as hydroxyl radicals (•OH) and superoxide radicals ($O_2•^-$), which play a crucial role in dye degradation.(Cai et al. 2017). The Mg 1s spectrum shows only one peak with binding energies of 1304.2 eV (MgO), 1304.1 eV (Zn-MgO), and 1304.1 eV (Sr-MgO), confirming the +2 oxidation state of Mg ions as illustrated in Fig. 7 b. In Fig. 7 d. representing the deep scan Zn 2p spectrum of Zn-MgO, different prominent peaks are observed at 1021.9eV (Zn 2p3/2) and 1044.8 eV (Zn 2p1/2), which are attributed to the Zn^{2+} ions. These peaks confirm the successful incorporation of Zn^{2+} ions into the MgO lattice [52]. The presence of Zn introduces defect states and modifies the electronic structure, facilitating charge separation and reducing electron-hole recombination during photocatalysis. The two peaks obtained with binding energies of 133.2 eV and 135 eV correspond to Sr-$d_{5/2}$ and Sr-$d_{3/2,}$ respectively, as shown in Fig. 7 e. A binding energy difference of 1.8 eV and coupling of spin orbitals confirm the incorporation of Sr ions into the MgO lattice (Shimi et al. 2022b). Owing to the larger ionic radius of Sr^{2+}, lattice distortion and defect formation are induced, which may promote charge -carrier mobility and enhance photocatalytic performance. The survey spectrum of MgO is displayed in Fig. 7a. The C 1s peaks observed at 285.1 eV indicate the adventitious carbon originating from atmospheric exposure and residual organic compounds associated with the plant-mediated synthesis process. Additionally, the peaks obtained at 88.9eV represent the core Mg-O linkages. As a result, the survey spectrum confirms the successful formation of MgO nanoparticles and incorporation of Zn and Sr dopants without detectable impurity phases.

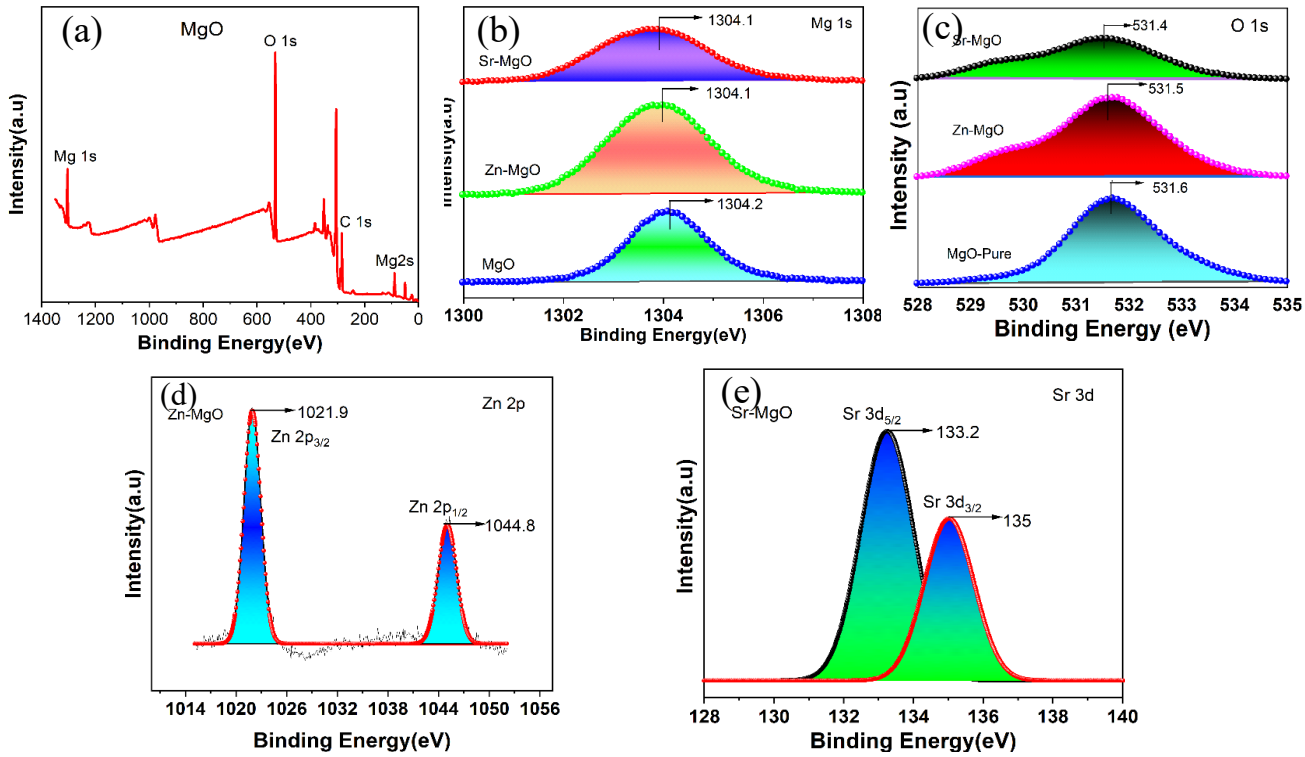


Fig.7. XPS studies (a) survey scan, (b) deconvolution spectrum of Mg 1s, (c) deep scan O1s spectrum, (d) deep scan Zn 2p spectrum, and (e) Sr 3d spectrum of ZS-doped MgO NPs

3.6 Photocatalytic activity of Methylene Blue

In recent years, photocatalytic methods have been developed for the degradation of organic pollutants such as dyes with an appropriate efficiency. The nanoparticles exhibit a higher surface area to volume ratio, which can increase the efficiency of the catalyst significantly when compared to the bulk materials. Particle size reduction can enhance the activity of the catalyst. In this present work, the green-synthesized MgO, Zn- and Sr-doped MgO NPs were examined for the methylene blue dye degradation with an absorption peak at 664nm under UV light irradiation and analyzed the photocatalytic efficiency. The prepared MB solutions at various concentrations (10, 20,35 and 50ppm) were examined at different pH levels (3, 6, 9 and 12), and various catalytic concentrations (5,20,35 and 50mg) of MgO, Zn-MgO and Sr-MgO NPs were measured at 15-minute time intervals up to 90minutes. The degradation efficiency was calculated by using Eq. (1). The kinetics of the dye degradation of methylene blue were determined from Eq. (8) (Shekofteh Narm et al. 2024)

$$\text{Kinetics } = \ln\frac{C_t}{C_0} = K_{obs} \quad 8$$

To optimize the degradation efficiency, various parameters, such as pH, MB dye concentrations, and the dosage of catalyst, were examined in the following

3.6.1. Effect of pH

The effect of solution on the photocatalytic degradation of methylene blue was investigated at pH values of 3, 6, 9, and 12 using an initial dye concentration of 10 ppm and a catalytic dosage of 50mg. The degradation efficiency of MB dye was measured by using Eq. (1), and the results are presented in Fig. 8. The pH of the solution is an important parameter because it influences the surface charge of the photocatalyst, the ionization state of the dye molecule, and the generation of reactive oxygen species during photocatalysis. The degradation efficiency was comparatively low for all photocatalysts at acidic pH 3. This behavior can be explained by the excess H^+ ions protonating the catalyst surface, which limits photocatalytic activity by reducing the availability of active sites and suppressing the generation of hydroxyl radicals (•OH).(Nguyen et al. 2019; Shimi et al. 2022b; Ahmad et al. 2025). The degradation efficiency improved steadily as the pH increased from 3 to 9, reaching its maximum at 88% for MgO, 94% for Zn-MgO, and 92% for Sr-MgO nanoparticles. The higher concentration of OH^- ions, which encourages the production of hydroxyl radicals, the primary oxidizing species responsible for MB degradation, is the fundamental cause of the enhanced degradation at alkaline pH. Additionally, in an alkaline environment, the negatively charged catalyst surface strengthens the contact with the cationic MB molecules, promoting photocatalytic oxidation. (Rani et al. 2025). Furthermore, the degradation efficiency of MgO, Zn-MgO, and Sr-MgO nanoparticles decreased slightly to 83%, 87%, and 86%, respectively, when the pH was raised to 12. Excessive OH^- ions occupying surface-active sites, increased charge-carrier recombination, and potential catalyst particle aggregation in very alkaline conditions are all potential causes of this drop in photocatalytic performance (Ahmad et al. 2025) as illustrated in Fig.8 (a2, b2, c2). These findings show that pH 9 is the optimum for efficient photocatalytic

degradation of MB dye by using the synthesized nanoparticles. The degradation efficiency of MB dye was further investigated through a kinetics study with correlation coefficients (R^2) of 0.99068, 0.9942, and 0.9914 for MgO, Zn-MgO, and Sr-MgO nanoparticles, respectively, confirming that the photocatalytic degradation process follows a pseudo-first-order model shown in Fig.8 (a3, b3, c3).

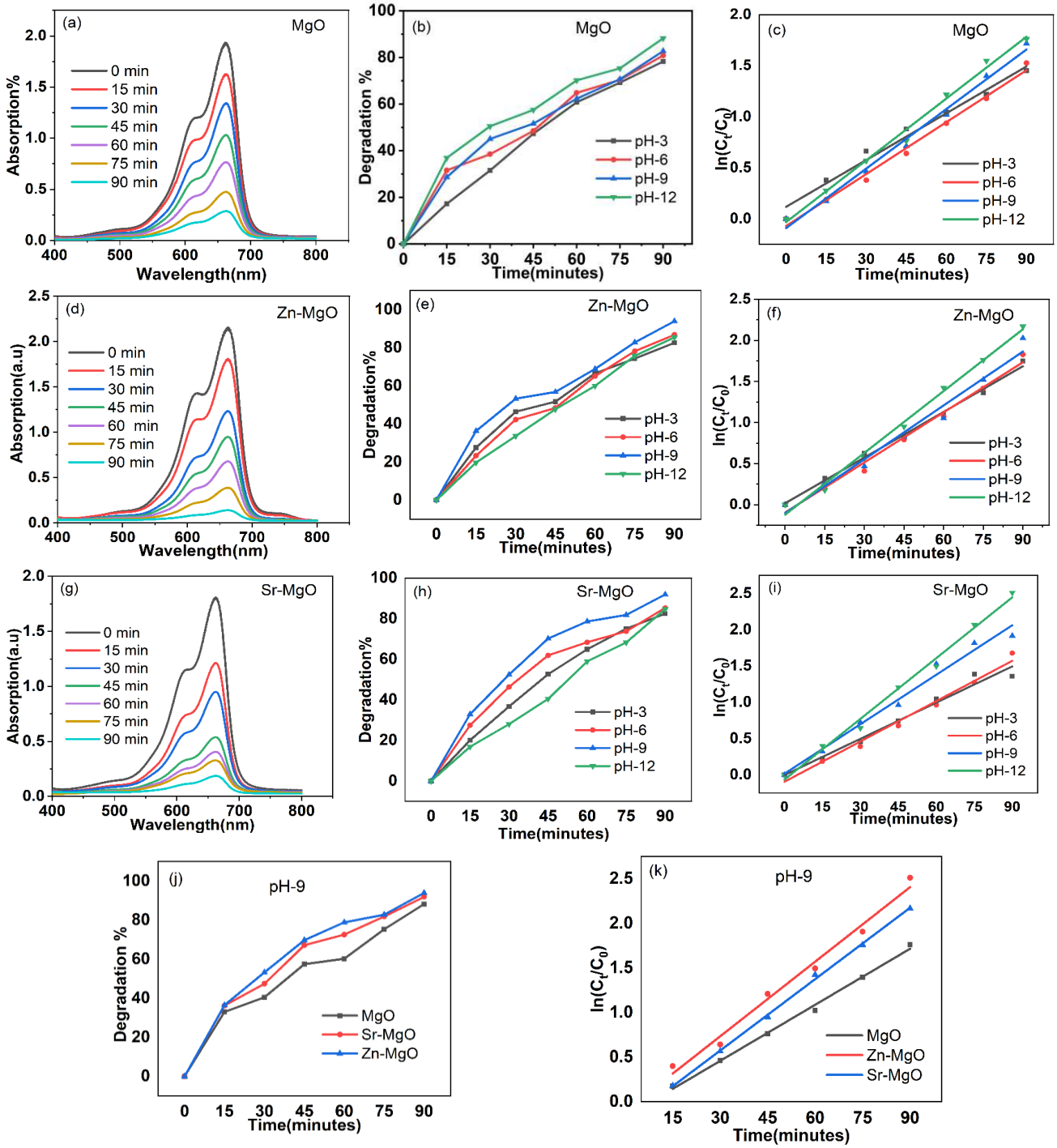


Fig.8.MB dye degradation % and kinetics of Zn- and Sr-doped MgO NPs (a-c) MgO, (d-f) Zn-MgO, (g-i) Sr-MgO, and (j & k) dye removal and kinetics at pH 9

3.6.2. Impact of dye concentration.

The impact of initial MB dye concentration on the photocatalytic removal of pure MgO, Zn-doped and Sr-doped MgO nanoparticles was investigated at pH 9 using a catalyst dosage of 50 mg and an irradiation time of 90 min. The dye concentration was varied from 10 to 50 mg; the corresponding degradation efficiencies are presented in Fig.9. The degradation efficiency decreased from 86.3% to 70% for MgO, from 94% to 77% for Zn-MgO, and from 93% to 73% for Sr-MgO nanoparticles as the dye concentration increased from 10 to 50 mg. At the lowest dye concentration (10 ppm), the maximum degradation efficiency was noted. Efficient adsorption and photocatalytic oxidation are made possible at lower concentrations because there are more active sites on the catalyst surface than there are dye molecules. Furthermore, light can enter the solution more efficiently, encouraging the production of reactive oxygen species and electron-hole pairs that cause dye degradation.(Nguyen et al. 2019). The degradation efficiency progressively dropped as the dye concentration increased. This decrease can be explained by more dye molecules saturating accessible active sites, which restricts the interaction between the pollutant and the photocatalyst. Additionally, the solution becomes more strongly colored at increased dye concentrations, which increases incident light absorption and scattering. As a result, fewer photons reach the catalyst surface, which lowers photocatalytic activity and charge-carrier production. Similar observations have been reported for the MgO-based photocatalysts Rani et al (Rani et al. 2025), Chen et al (Chen et al. 2019) and Jawad et al (Jawad et al. 2023). Among the synthesized photocatalysts, Zn-doped MgO exhibited the highest degradation efficiency at all investigated dye concentrations, which can be attributed to its reduced band-gap energy and enhanced light-harvesting capability. The photocatalytic degradation process followed pseudo-first-order kinetics, with correlation coefficients (R^2) of 0.9903, 0.9900, and 0.9975 for MgO, Zn-MgO, and Sr-MgO nanoparticles,

respectively, confirming the applicability of the first-order kinetic model represented in Fig.9 (a_3-d_3).

3.6.3. Impact of catalytic dosage

The impact of catalytic dosage on the photocatalytic degradation of methylene blue dye removal was examined using MgO, Zn- doped MgO and Sr-doped MgO nanoparticles at catalytic loading of 5, 20, 35 and 50 mg. The studies were conducted under 90 minutes of radiation using a 10-ppm MB solution at pH 9, and the results are shown in Fig.10. The degradation efficiency increased as the catalyst dosage was raised from 5 to 35 mg. The degrading efficiency for pure MgO improved from 72% to 89%, while Zn-doped MgO and Sr-doped MgO nanoparticles showed increases from 79% to 95% and 78% to 94%, respectively. The enhanced degradation performance at higher catalyst loading can be attributed to an increased number of available active sites and a larger effective surface area, which encourage dye molecule adsorption and facilitate the production of reactive oxygen species (ROS), such as hydroxyl radicals (•OH) and superoxide radicals ($O_2^{\bullet -}$), which are responsible for the improved degradation performance at higher catalyst loading. As a result, the degradation process involves more photogenerated charge carriers, which enhance photocatalytic activity.(Gebreaneniya et al. 2024). Conversely, the degradation efficiency decreased when the catalyst dosage was increased to 50 mg. For MgO, Zn-doped MgO, and Sr-doped MgO nanoparticles, the degradation efficiency dropped to 79%, 85%, and 80%, respectively. Excessive catalyst loading, which raises suspension turbidity and decreases light penetration through the reaction medium, may be the cause of this reduction. Moreover, at higher catalyst concentrations, particle agglomeration might limit the production of reactive oxygen species and diminish photocatalytic effectiveness by reducing the effective surface area and blocking active sites. Prior research on metal oxide photocatalysts has revealed similar findings. (S R et al. 2018). Among the photocatalysts, Zn-doped MgO showed the best degradation efficiency across all catalyst doses among the examined photocatalysts. This better performance is in line

with the XPS study, which verified successful Zn incorporation and a change in the surface electronic structure, and the UV-DRS data, which showed a lower band-gap energy (2.31 eV). These elements boost photocatalytic degradation efficiency, enable charge-carrier separation, and increase light absorption. Correlation values (R^2) for MgO, Zn-doped MgO, and Sr-doped MgO nanoparticles were 0.9951, 0.9919, and 0.9908, respectively, indicating pseudo-first-order kinetics in the photocatalytic degradation process. The strong R2 values verify the efficacy of the produced photocatalysts for MB degradation and show good agreement with the first-order kinetic model, as shown in Fig.10 (a_3-d_3).

The optimum catalyst loading for MgO, Zn-doped MgO, and Sr-doped MgO nanoparticles was determined to be 35 mg based on the catalyst dose optimization study. Maximum degradation efficiencies of 89%, 95%, and 94%, respectively, were attained at this dosage. Degradation efficiency decreased when the catalyst dosage was raised to 50 mg because of increased light scattering and particle aggregation. Consequently, the ideal catalyst dosage for further photocatalytic studies was determined to be 35 mg.

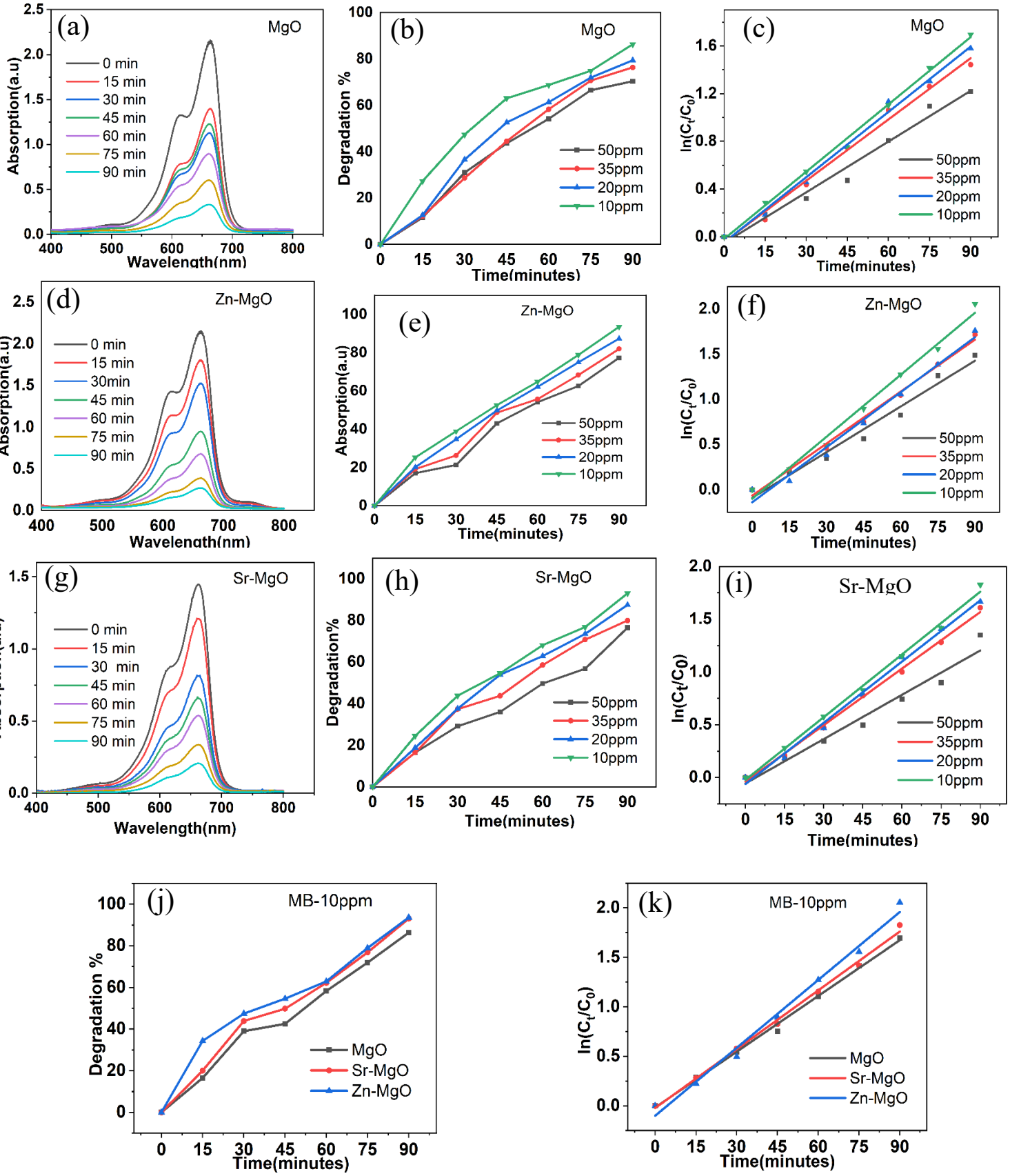

(a)
MgO
0 min
15 min
30 min
45 min
60 min
75 min
90 min
Absorption(a.u)
Wavelength(nm)
(b)
MgO
50ppm
35ppm
20ppm
10ppm
Degradation %
Time(minutes)
(c)
MgO
50ppm
35ppm
20ppm
10ppm
ln(C_t/C_0)
Time(minutes)
(d)
Zn-MgO
0 min
15 min
30min
45 min
60 min
75 min
90 min
Absorption(a.u)
Wavelength(nm)
(e)
Zn-MgO
50ppm
35ppm
20ppm
10ppm
Absorption(a.u)
Time(minutes)
(f)
Zn-MgO
50ppm
35ppm
20ppm
10ppm
ln(C_t/C_0)
Time(minutes)
(g)
Sr-MgO
0 min
15 min
30 min
45 min
60 min
75 min
90 min
Absorption(a.u)
Wavelength(nm)
(h)
Sr-MgO
50ppm
35ppm
20ppm
10ppm
Degradation%
Time(minutes)
(i)
Sr-MgO
50ppm
35ppm
20ppm
10ppm
ln(C_t/C_0)
Time(minutes)
(j)
MB-10ppm
MgO
Sr-MgO
Zn-MgO
Degradation %
Time(minutes)
(k)
MB-10ppm
MgO
Sr-MgO
Zn-MgO
ln(C_t/C_0)
Time(minutes)

Fig.9.MB dye degradation % and kinetics of Zn- and Sr-doped MgO NPs with various dye concentrations (a-c) MgO, (d-f) Zn-MgO, (g-i) Sr-MgO, and (j & k) dye removal and kinetics at 10ppm MB

3.6.4. Impact of doping

The photocatalytic degradation efficiency of methylene blue has improved upon the addition of Zn and Sr ions to the MgO lattice. The combined impacts of the dopant ions' structural and electrical changes are responsible for the enhanced photocatalytic performance. According to UV-DRS research, the band-gap energy dropped from 3.59 eV for pure MgO to 2.31 eV and 2.57 eV for MgO nanoparticles doped with Zn and Sr, respectively. By extending the light absorption range toward the visible area, the decrease in band-gap energy improved the production of photogenerated charge carriers and allowed for more effective use of incident irradiation. Moreover, charge-carrier separation and electron-hole recombination were inhibited by the addition of Zn and Sr dopant ions to the MgO lattice. Additionally, XPS examination revealed changes in the surface electronic environment and verified the successful incorporation of Zn^{2+} and Sr^{2+} ions into the MgO lattice. In order to promote charge-carrier migration and inhibit electron-hole recombination, the dopant ions introduce defect sites and localized energy states. Consequently, more photogenerated electrons and holes contribute to the production of reactive oxygen species, including superoxide radicals ($O_2^{\bullet-}$) and hydroxyl radicals (•OH), which break down methylene blue molecules.(Yousefi et al. 2015) Furthermore, XRD examination showed that following doping, the crystallite size decreased from 15.6 nm for pure MgO to 11.2 nm and 12.85 nm for Zn-doped and Sr-doped MgO nanoparticles, respectively. By shortening the charge-carrier diffusion path and increasing the number of accessible surface-active sites, the smaller crystallite size improves photocatalytic efficiency.(Kumar 2017; Shkir et al. 2024a). Based on the results, Zn-doped MgO showed the highest degradation efficiency among the produced photocatalysts, which can be explained by its smaller crystallite size, lower band-gap energy, and better charge separation properties.

Thus, the improved charge-carrier separation, reduced crystallite size, defect production, and band-gap narrowing all collectively contributed to the superior photocatalytic performance of the doped MgO nanoparticles, as represented in Table 3

The aforementioned findings clearly indicated that the photocatalytic activity of methylene blue dye was determined by various parameters such as pH, dye concentrations, catalytic concentrations, surface area, irradiation time, size, dopant ions, and the nature of the dyes. These variables determine the photocatalytic degradation percentage. Table 4 compares the photocatalytic performance of the synthesized nanoparticles with previously reported photocatalysts for methylene blue degradation.

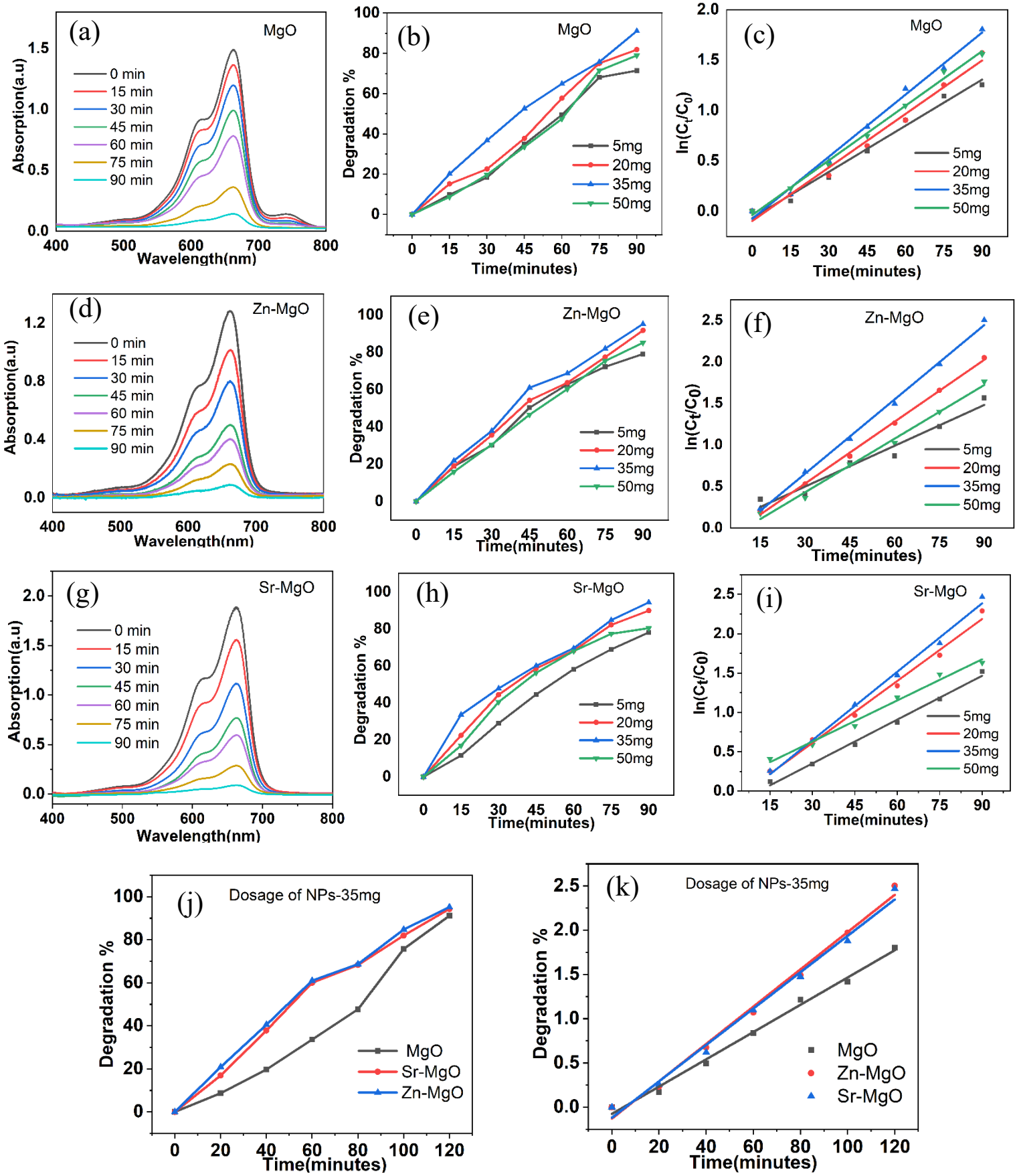


Fig.10. MB dye degradation % and kinetics of Zn- and Sr-doped MgO NPs with various catalytic concentrations (a-c) MgO, (d-f) Zn-MgO, (g-i) Sr-MgO, and (j & k) dye removal and kinetics at 35mg of nanoparticles.

Table 3. Photocatalytic dye removal efficiency of MB dye by doping of Zn- and Sr-doped MgO nanoparticles at different parameters.

Nanoparticles	Degradation percentage			
	pH-9	Dye concentration (10ppm)	Catalytic concentration (35mg)	Time (mins)
MgO	88%	86%	89%	90
Zn-doped MgO	94%	94%	95%	90
Sr-doped MgO	92%	93%	94%	90

3.7. Photocatalytic degradation mechanism

Figure 11 depicts the suggested photocatalytic degradation pathway of methylene blue (MB) over MgO, Zn-doped MgO, and Sr-doped MgO nanoparticles under light irradiation. During the irradiation time, the synthesized photocatalysts were exposed to UV light. The absorbed energy is higher than the bandgap energy (Eg), electrons are promoted to the conduction band (CB) from the valence band (VB) of the catalyst, resulting in the formation of holes (h_{VB}^{+}) in the valence band and electrons (e^{-}_{CB}) created at the conduction band. During the process, holes (h^{+}) in the VB combine with H_2O molecules to generate hydroxyl radicals (OH), which act as strong oxidants, while electrons (e-) in the CB are involved in reduction with O2 molecules to create superoxide anions (O^{2-}), which operate as a powerful reducer. Additionally, hydrogen peroxide (H_2O_2) is further produced by superoxide anions (O_2^-). Finally, more active species such as hydroxyl radicals ($OH^{\bullet}$), superoxide anions (O_2^-) and hydrogen peroxide (H_2O_2) quickly react with MB dye, undergoing decomposition through the splitting of the bond between carbon-carbon, carbon-hydrogen and carbon-sulfur, resulting in the methylene dye molecules being degraded into CO_2, H_2O and some byproducts such as NH_4^+, NO_3^-, Cl^- and SO_2^- (Shimi et al. 2022b; Loke et al. 2022; Shekofteh Narm et al. 2024; Khan et al. 2024). Overall, the reaction mechanism of MB is summarised as follows.

$$MgO + hv \longrightarrow MgO\ (e^{-}_{CB} + h^{+}_{VB})$$

$$h^{+}_{VB} + H_2O \longrightarrow OH^{\bullet} + H^{+} \text{(formation of hydroxyl radicals)}$$

$$e^{-}_{VB} + O_2 \longrightarrow O^{2-} \text{(formation of superoxide anions)}$$

$$O^{2-} + 2H^{+} + e^{-} \longrightarrow H_2O_2 \text{(formation of hydrogen peroxide)}$$

$$OH^{\bullet} + O^{2-} + H_2O_2 + (MB)C_{16}H_{18}ClN_3S \longrightarrow CO_2 + H_2O + NH_4^{+} + NO_3^{-} + Cl^{-} + SO_2^{-}$$

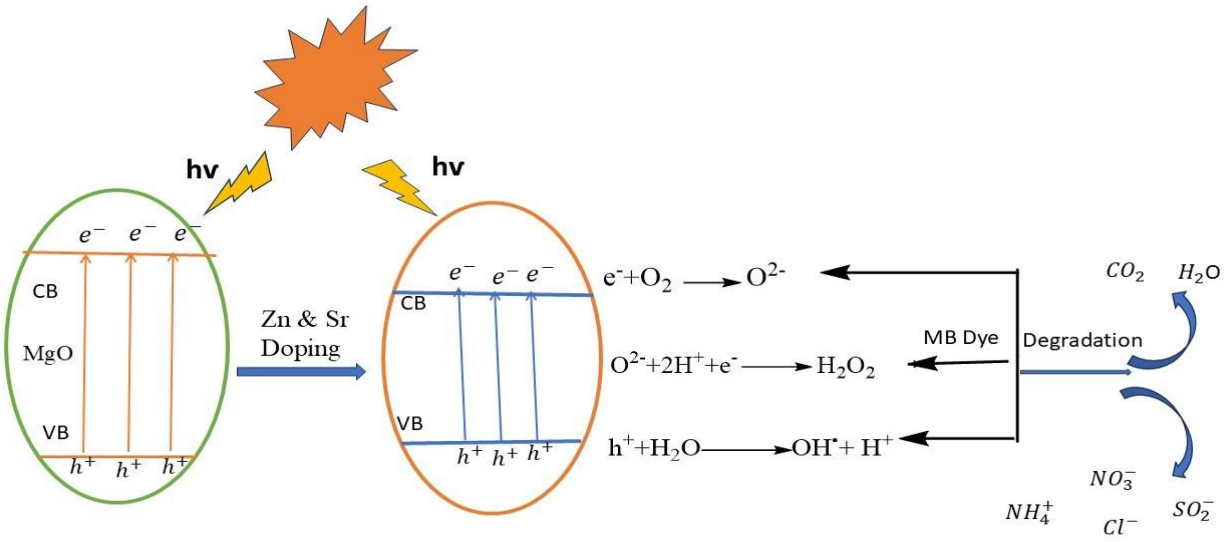


Fig.11.Schematic diagram for the mechanism of photocatalytic degradation of MB dye by using ZS- doped MgO nanoparticles

3.7.1 Recyclability and stability

Recyclability experiments were carried out under optimal conditions, using ZS-doped MgO NPs for methylene blue degradation to assess the catalysts' long-term performance. Following each cycle, the catalyst was recovered by centrifugation, repeatedly rinsed with double-distilled water to remove any adsorbed colour molecules, and then dried at 100 °C before reuse. After four consecutive cycles, the degradation efficiency was observed from 78 % for MgO, 86 % for Zn-MgO and 85 % for Sr-MgO, showing just a little decline in degradation efficiency, indicating their robust resistance to deactivation are shown in Fig.12. This stability implies that MgO and its doped MgO NPs can be used as efficient photocatalysts for sustainable wastewater cleanup and have dependable reusability.

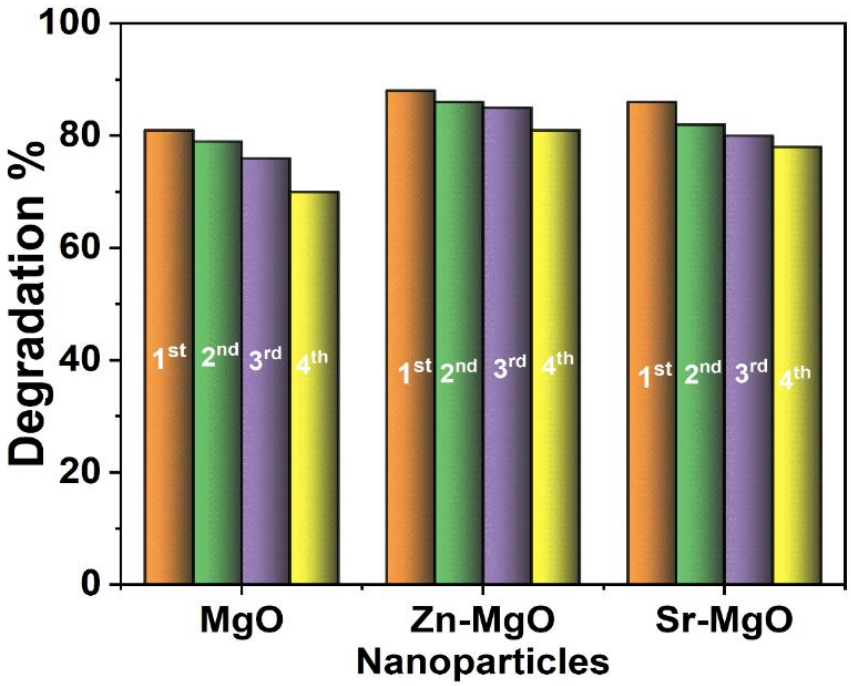


Fig.12. Recyclability and stability of ZS- doped MgO nanoparticles for 1st -4th cycles

Table 4. Photocatalytic dye removal percentage of MB by using various doped nanoparticles

Nanoparticles	Degradation time	Synthesis method	Plant extract	Degradation %	Ref
MgO	250 mins	Green synthesis	Dalbergia sissoo leaf	81%	(Khan et al. 2024)
MgO	160 mins	Green synthesis	date pits	64%	(Sackey et al. 2020)
MgO	110 mins	Green synthesis	Hyphaene thebaica	98%	(Muhaymin et al. 2024)
MgO	120 mins	Green synthesis	Chitosan polymer	87%	(Jawad et al. 2023)
MgO	120 mins	Chemical Synthesis	-	75%	(Balakrishnan et al. 2020)

MgO	180 mins	Chemical method	-	83%	(Tlili et al. 2021)
Ag-MgO	180 mins	Solgel	-	75%	(Alaizeri et al. 2021)
Ag-doped ZnO/MgO	120 mins	Green synthesis	Mentha pulegium	98%	(Shekofteh Narm et al. 2024)
Ni-MgO	60 mins	Green synthesis	Synadenium grantii	94%	(Purushotham 2025)
Cu-MgO	150 mins	Solgel	-	90%	(Subash et al. 2022)
Sr-ZnO	120 mins	Solgel	-	78.5%	(Yousefi et al. 2015)
Co-MgO	60 mins	Green synthesis	Neem leaves	91%	(Jeena et al. 2023)
Pure-MgO Zn-MgO Sr-MgO	90 mins	Green synthesis	Solanum torvum	MgO-89% Zn-MgO-95% Sr-MgO-94%	Present study

4. Conclusion

The objective of the present study is to synthesise ZS-doped MgO nanoparticles by using *S.torvum* plant leaf extract. The green approach is cost-effective and an environmentally friendly technique compared to various existing traditional approaches. *Solanum torvum* plant leaf extract acts as an efficient capping and stabilising agent for controlling the shape and

growth of MgO NPs. The green-synthesized MgO and doped MgO nanoparticles were characterized by XRD, FT-IR, UV-DRS, SEM with EDX, HRTEM, and XPS. In XRD analysis, it was confirmed that the pure MgO and doped MgO nanoparticles have a face-centered cubic structure. The stretching vibrations represent the presence of the Mg-O bond, and the plant leaf extract contains various phytochemical groups, which contribute to the reduction and stabilization of the nanoparticles, as confirmed by the FT-IR spectrum. Optical analysis revealed a band gap tailored from 3.59eV (pure MgO) to 2.31eV (Zn-MgO) and 2.57 eV (Sr-MgO) upon doping, confirmed by UV-DRS. The SEM results showed that the MgO nanoparticles are irregular in shape and form small agglomerations; the EDX spectrum confirms the dispersion of Zn and Sr into the MgO lattice. XPS analysis further confirms the chemical state of Mg, Zn, Sr, and lattice oxygen. The average particle size of the nanoparticles decreased from 14nm (MgO) to 11nm (Zn-MgO) and 12.6nm (Sr-MgO), while doping was confirmed by the HRTEM histogram. The dye removal efficiency of methylene blue was examined on pure MgO, Zn-MgO, and Sr-MgO nanoparticles with various dye concentrations, different pH values, and varying catalytic concentrations under UV light irradiation. The photocatalytic efficiency is observed to be 88% for MgO, 94% for Zn-MgO, and 92% for Sr-MgO at pH 9. The degradation percentage is 86% (MgO), 94% (Zn-MgO), and 93% (Sr-MgO) at 10ppm of methylene blue dye. The maximum dye degradation percentage was found at 35mg of catalyst dosage: 89% for MgO, 95% for Zn-MgO, and 94% for Sr-MgO. The results indicate that Zn- and Sr-doped MgO nanoparticles have better photocatalytic activity than pure MgO NPs, due to doping widening the band gap of the nanoparticles. The kinetics of the photocatalytic reaction for MB dye removal were a first-order reaction. According to the results, it is observed that the green synthesis of MgO nanoparticles, pure and doped using *Solanum torvum* plant leaf extract, might provide significant applications in wastewater treatment for the decomposition of cationic dyes.

Declaration of competing interests

The authors declare that they have no known competing financial interests or personal relationships that could have appeared to influence the work reported in this paper.

Acknowledgment

The authors would like to express their gratitude to the Department of Chemistry, Knowledge Institute of Technology, Salem, Paavai Engineering College, Namakkal, and Chemkovil Laboratory, Salem, Tamil Nadu, India, for providing the necessary facilities for conducting the research.

References

Ahmad H, Siddique AB, Zaheer S, et al (2025) Energy bandgap tuning of Sr-doped ZnO nanoparticles for photodegradation of azo dyes and antibacterial applications. J Water Process Eng 74:107855. https://doi.org/https://doi.org/10.1016/j.jwpe.2025.107855

Alaizeri ZM, Alhadlaq HA, Aldawood S, et al (2021) Facile Synthesis, Characterization, Photocatalytic Activity, and Cytotoxicity of Ag-Doped MgO Nanoparticles. Nanomaterials 11:2915

Aldawsari AM, Alsohaimi I, Hassan HMA, et al (2021) Tailoring an efficient nanocomposite of activated carbon-layered double hydroxide for elimination of water-soluble dyes. J Alloys Compd 857:157551. https://doi.org/https://doi.org/10.1016/j.jallcom.2020.157551

Almontasser A, Parveen A (2022) Probing the effect of Ni, Co and Fe doping concentrations on the antibacterial behaviors of MgO nanoparticles. Sci Rep 12:. https://doi.org/10.1038/s41598-022-12081-z

Ayvacikli M, Kaynar ÜH, Karabulut Y, et al (2020) Synthesis and photoluminescence characteristics of Dy incorporated MoO3 phosphor: Suppression concentration quenching. Appl Radiat Isot 164:. https://doi.org/10.1016/j.apradiso.2020.109321

Balakrishnan G, Ramasamy V, Batoo K, Raslan E (2020) Microstructure, Optical and Photocatalytic Properties of MgO Nanoparticles. Results Phys 16:103013. https://doi.org/10.1016/j.rinp.2020.103013

Barzegar M, Ahmadvand D, Sabouri Z, Darroudi M (2023) Green synthesis of magnesium oxide nanoparticles by chitosan polymer and assessment of their photocatalytic activity and cytotoxicity influences. Mater Chem Phys 301:127649. https://doi.org/https://doi.org/10.1016/j.matchemphys.2023.127649

Benisha R, M A, Mani A, et al (2022) Catharanthus roseus leaf extract mediated Ag-MgO nanocatalyst for Photocatalytic degradation of congo red dye and their antibacterial activity. J Mol Struct 1262:133005. https://doi.org/10.1016/j.molstruc.2022.133005

Cai Y, Li C, Wu D, et al (2017) Highly active MgO nanoparticles for simultaneous bacterial inactivation and heavy metal removal from aqueous solution. Chem Eng J 312:158–166. https://doi.org/https://doi.org/10.1016/j.cej.2016.11.134

Chauhan D, Kumar R, Thakur N, et al (2024) Ocimum sanctum-mediated co/cu/zn-doped magnesium oxide nanoparticles: Photocatalytic, antibacterial, and antioxidant properties for environmental remediation. Hybrid Adv 6:100199. https://doi.org/https://doi.org/10.1016/j.hybadv.2024.100199

Chayed NF, Kamarulzaman N, Badar N, Elong K (2019) Effect of Cu Doped in MgO on Nanostructures and their Band Gap Energies. Solid State Phenom 290:323–328.

https://doi.org/10.4028/www.scientific.net/SSP.290.323

Chen J, Wang X, Huang Y, et al (2019) Adsorption Removal of Pollutant Dyes in Wastewater by Nitrogen-doped Porous Carbons Derived from Natural Leaves . Eng. Sci. 5:30–38

D'Souza JN, Nagaraja GK, Meghana Navada K, et al (2021) Insight into the impact of zinc doping on the structural, surface, and biological properties of magnasium oxide nanoparticles stabilized by Vateria indica (L.) fruit extract. Ceram Int 47:29620–29630. https://doi.org/https://doi.org/10.1016/j.ceramint.2021.07.131

Endla P (2025) Synthesis, Structural Characterization, and Enhanced Photocatalytic Activity of Ni-Doped Magnesium Oxide Nanoparticles Using Synadenium Grantii Extract. J Inorg Organomet Polym Mater 1–18. https://doi.org/10.1007/s10904-025-03938-7

Fouda A, Hassan SE-D, Saied E, Hamza MF (2021) Photocatalytic degradation of real textile and tannery effluent using biosynthesized magnesium oxide nanoparticles (MgO-NPs), heavy metal adsorption, phytotoxicity, and antimicrobial activity. J Environ Chem Eng 9:105346. https://doi.org/https://doi.org/10.1016/j.jece.2021.105346

Gebreaneniya M, Berhe GG, Gebretsadik T (2024) Synthesis, Characterization, and Photocatalytic Activity of Cu-Doped MgO Nanoparticles on Degradation of Methyl Orange (MO). Adv Mater Sci Eng 2024:1–10. https://doi.org/10.1155/2024/9969064

Gong Y, Tang J, Zhao D (2016) Application of iron sulfide particles for groundwater and soil remediation: A review. Water Res 89:309–320. https://doi.org/10.1016/j.watres.2015.11.063

Hassan HMA, El-Aassar MR, El-Hashemy MA, et al (2022) Sulfanilic acid-functionalized magnetic GO as a robust adsorbent for the efficient adsorption of methylene blue from aqueous solution. J Mol Liq 361:119603. https://doi.org/https://doi.org/10.1016/j.molliq.2022.119603

Hornak J (2021) Synthesis, Properties, and Selected Technical Applications of Magnesium Oxide Nanoparticles: A Review. Int. J. Mol. Sci. 22:12752

Hotan Alsohaimi I, Alhumaimess MS, Abdullah Alqadami A, et al (2023) Adsorptive performance of aminonaphthalenesulfonic acid modified magnetic-graphene oxide for methylene blue dye: Mechanism, isotherm and thermodynamic studies. Inorg Chem Commun 147:110261. https://doi.org/https://doi.org/10.1016/j.inoche.2022.110261

Jawad AH, Abdulhameed AS, Surip SN, Alothman ZA (2023) Hybrid multifunctional biocomposite of chitosan grafted benzaldehyde/montmorillonite/algae for effective removal of brilliant green and reactive blue 19 dyes: Optimization and adsorption mechanism. J Clean Prod 393:136334. https://doi.org/https://doi.org/10.1016/j.jclepro.2023.136334

Jeena T, Geetha MP, Suchetan PA, et al (2023) Influence of cobalt doping on chemical and green synthesized magnesium oxide nanoparticles for enhanced photocatalytic evaluation, adsorption studies, antimicrobial analysis and corrosion inhibition study. Inorg Chem Commun 157:111232. https://doi.org/https://doi.org/10.1016/j.inoche.2023.111232

Kalam A, Al-Sehemi AG, Assiri M, et al (2018) Modified solvothermal synthesis of cobalt ferrite (CoFe2O4) magnetic nanoparticles photocatalysts for degradation of methylene blue with H2O2/visible light. Results Phys 8:1046–1053. https://doi.org/https://doi.org/10.1016/j.rinp.2018.01.045

Kandasamy N, Shanmugam P, Parasuraman B, et al (2026) Boosting photodegradation performance through efficient MnO2/rGO nanocomposite: water remediation application. J Sol-Gel Sci Technol 117:. https://doi.org/10.1007/s10971-025-07093-w

Khan S, Noor T, Iqbal N, Yaqoob L (2024) Photocatalytic Dye Degradation from Textile Wastewater: A Review. ACS Omega 9:21751–21767. https://doi.org/10.1021/acsomega.4c00887

Kumar A (2017) A Review on the Factors Affecting the Photocatalytic Degradation of Hazardous Materials. Mater Sci Eng Int J 1:. https://doi.org/10.15406/mseij.2017.01.00018

Kuruthukulangara N, Asharani I (2023) Photocatalytic degradation of Rhodamine B a carcinogenic pollutant by MgO nanoparticles. Inorg Chem Commun 160:111873. https://doi.org/10.1016/j.inoche.2023.111873

Kuruthukulangara N, Asharani I V. (2024) Photocatalytic degradation of Rhodamine B, a carcinogenic pollutant, by MgO nanoparticles. Inorg Chem Commun 160:111873. https://doi.org/10.1016/j.inoche.2023.111873

Li Z, Yang Y, Dai K, et al (2019) Construction of defective Mo 15 S 19 /CdS-diethylenetriamine heterosctructure photocatalyst for highly active and stable noble-metal-free photocatalytic hydrogen production. Appl Surf Sci 469:505–513. https://doi.org/10.1016/j.apsusc.2018.11.078

Lin Q, Zeng G, Yan G, et al (2022) Self-cleaning photocatalytic MXene composite membrane for synergistically enhanced water treatment: Oil/water separation and dyes removal. Chem Eng J 427:131668. https://doi.org/https://doi.org/10.1016/j.cej.2021.131668

Loke JY, Zaki RS, Setiabudi H (2022) Photocatalytic degradation of methylene blue using ZnO supported on wood waste-derived activated carbon (ZnO/AC). Mater Today Proc 57:. https://doi.org/10.1016/j.matpr.2021.12.535

Mahala S, Arumugam SM, Kumar S, et al (2023) Tuning of MgO's base characteristics by blending it with amphoteric ZnO facilitating the selective glucose isomerization to

fructose for bioenergy development. Nanoscale Adv 5:2470–2486. https://doi.org/10.1039/D3NA00097D

Makuła P, Pacia M, Macyk W (2018) How To Correctly Determine the Band Gap Energy of Modified Semiconductor Photocatalysts Based on UV–Vis Spectra. J Phys Chem Lett 9:6814–6817. https://doi.org/10.1021/acs.jpclett.8b02892

Mohan AC, Athira A, Nair BP, et al (2024) Multifaceted properties of Ni and Zn codoped MgO nanoparticles. Sci Rep 14:32067. https://doi.org/10.1038/s41598-024-83779-5

Muhaymin A, Mohamed HEA, Hkiri K, et al (2024) Green synthesis of magnesium oxide nanoparticles using Hyphaene thebaica extract and their photocatalytic activities. Sci Rep 14:20135. https://doi.org/10.1038/s41598-024-71149-0

Nadimi M, Ziarati A, Aroon M, Ebrahimian Pirbazari A (2018) Photodegradation of Methylene Blue by a ternary magnetic TiO2/Fe3O4/Graphene oxide nanocomposite under visible light. Mater Chem Phys 225:. https://doi.org/10.1016/j.matchemphys.2018.11.029

Namakka M, Rahman MR, Said KAM Bin, et al (2023) A review of nanoparticle synthesis methods, classifications, applications, and characterization. Environ Nanotechnology, Monit Manag 20:100900. https://doi.org/https://doi.org/10.1016/j.enmm.2023.100900

Naren Vidaarth TM, Surendhiran S, Jagan KSG, et al (2024) Surface chemistry of phytochemical enriched MgO nanoparticles for antibacterial, antioxidant, and textile dye degradation applications. J Photochem Photobiol A Chem 448:115349. https://doi.org/10.1016/j.jphotochem.2023.115349

Nguyen LTT, Nguyen LTH, Duong ATT, et al (2019) Preparation, Characterization and Photocatalytic Activity of La-Doped Zinc Oxide Nanoparticles. Materials (Basel). 12:1195

Panchal P, Meena P, Nehra SP (2021) A rapid green synthesis of Ag/AgCl-NC photocatalyst for environmental applications. Environ Sci Pollut Res 28:3972–3982. https://doi.org/10.1007/s11356-020-11834-5

Patil P, Nerlekar N, Kuldeep A, et al (2024) Terminalia bellirica (Gaertn.) Roxb. extract-mediated green synthesis of magnesium oxide nanoparticles for multifunctional applications. Plant Nano Biol 8:100069. https://doi.org/10.1016/j.plana.2024.100069

Paul DR, Sharma R, Panchal P, et al Silver Doped Graphitic Carbon Nitride for the Enhanced Photocatalytic Activity Towards Organic Dyes. J. Nanosci. Nanotechnol. 19:5241–5248

Pugazhendhi S, Jayavel R (2023) Synthesis of Solanum torvum (Solanaceae) mediated silver nanoparticles and their nonlinear characterizations. Inorg Chem Commun 156:111129. https://doi.org/https://doi.org/10.1016/j.inoche.2023.111129

Purushotham E (2025) Synthesis , Structural Characterization , and Enhanced Photocatalytic

Activity of Ni-Doped Magnesium Oxide Nanoparticles Using Synadenium Grantii Extract

Rajendran V, Deepa B, Mekala R (2018) Studies on structural, morphological, optical and antibacterial activity of Pure and Cu-doped MgO nanoparticles synthesized by co-precipitation method. Mater Today Proc 5:8796–8803. https://doi.org/https://doi.org/10.1016/j.matpr.2017.12.308

Ramanujam K, Sundrarajan M (2014) Antibacterial effects of biosynthesized MgO nanoparticles using ethanolic fruit extract of Emblica officinalis. J Photochem Photobiol B Biol 141:296–300. https://doi.org/https://doi.org/10.1016/j.jphotobiol.2014.09.011

Rani S, Kumar P, Kataria N (2025) Development of chemically and green synthesized MgO nanoparticles for CR and BG dye adsorption from single and binary aqueous system. J Taiwan Inst Chem Eng 166:105566. https://doi.org/https://doi.org/10.1016/j.jtice.2024.105566

Ruíz-Baltazar Á de J, Reyes-López SY, Mondragón-Sánchez M de L, et al (2019) Eco-friendly synthesis of Fe3O4 nanoparticles: Evaluation of their catalytic activity in methylene blue degradation by kinetic adsorption models. Results Phys 12:989–995. https://doi.org/https://doi.org/10.1016/j.rinp.2018.12.037

S R S, Madhu G, Hashir M (2018) Studies on Nano-Engineered TiO 2 Photo Catalyst for Effective Degradation of Dye. IOP Conf Ser Mater Sci Eng 310:12026. https://doi.org/10.1088/1757-899X/310/1/012026

Saadabadi RH, Tehrani FS, Sabouri Z, Deionized DI (2024) Photocatalytic activity and anticancer properties of green nanocomposite via Ocimum basilicum L . seed extract. 1–17

Sackey J, Bashir AKH, Ameh A, et al (2020) Date pits extracts assisted synthesis of Magnesium Oxides Nanoparticles and its application towards the photocatalytic degradation of methylene blue. J King Saud Univ - Sci 32:. https://doi.org/10.1016/j.jksus.2020.06.013

Saleh NB, Milliron DJ, Aich N, et al (2016) Importance of doping, dopant distribution, and defects on electronic band structure alteration of metal oxide nanoparticles: Implications for reactive oxygen species. Sci Total Environ 568:926–932. https://doi.org/10.1016/j.scitotenv.2016.06.145

Shah AA, Jayalakshmi D, Xavier B (2021) Characterization of gold nanoparticles synthesized from Solanum torvum (Turkey Berry) fruit extract and its application in catalytic degradation of methylene blue and antibacterial properties. Mater Today Proc 47:927–932. https://doi.org/https://doi.org/10.1016/j.matpr.2021.04.606

Shahzadi S, Fatima S, ul ain Q, et al (2025) A review on green synthesis of silver nanoparticles (SNPs) using plant extracts: a multifaceted approach in photocatalysis, environmental remediation, and biomedicine. RSC Adv 15:3858–3903. https://doi.org/10.1039/D4RA07519F

Shanmugam J, Sharmili Sundararaj A, Shanmugasundaram R, et al (2023) Green preparation of bract extract (Musa acuminate) doped magnesium oxide nanoparticles and their bioefficacy. Appl Organomet Chem 37:e7063. https://doi.org/https://doi.org/10.1002/aoc.7063

Shekofteh Narm T, Hamidinezhad H, Sabouri Z, Darroudi M (2024) Green synthesis of silver doped zinc oxide/magnesium oxide nanocomposite for waste water treatment and examination of their cytotoxicity properties. Heliyon 10:e30374. https://doi.org/10.1016/j.heliyon.2024.e30374

Shimi AK, Parvathiraj C, Kumari S, et al (2022a) Green synthesis of SrO nanoparticles using leaf extract of Albizia julibrissin and its recyclable photocatalytic activity: an eco-friendly approach for treatment of industrial wastewater. Environ Sci Adv 1:849–861. https://doi.org/10.1039/D2VA00018K

Shimi AK, Parvathiraj C, Kumari S, Dalal J (2022b) Green synthesis of SrO nanoparticles using leaf extract of Albizia julibrissin and its recyclable photocatalytic activity : an eco-friendly approach. 849–861. https://doi.org/10.1039/d2va00018k

Shkir M, AlAbdulaal TH, Manthrammel MA, Khan FS (2024a) Novel MgO and Ag/MgO nanoparticles green-synthesis for antibacterial and photocatalytic applications: A kinetics-mechanism & recyclability. J Photochem Photobiol A Chem 449:115398. https://doi.org/https://doi.org/10.1016/j.jphotochem.2023.115398

Shkir M, AlAbdulaal TH, Manthrammel MA, Khan FS (2024b) Novel MgO and Ag/MgO nanoparticles green-synthesis for antibacterial and photocatalytic applications: A kinetics-mechanism & recyclability. J Photochem Photobiol A Chem 449:115398. https://doi.org/10.1016/j.jphotochem.2023.115398

Singh PK, Singh N, Singh M, et al (2021) Fabrication of nanostructured MgO and Zn-doped MgO as an efficient LPG sensing materials operable at room temperature. Appl Phys A 127:563. https://doi.org/10.1007/s00339-021-04712-5

Srinivasan L V., Rana SS (2024) A critical review of various synthesis methods of nanoparticles and their applications in biomedical, regenerative medicine, food packaging, and environment. Discov Appl Sci 6:. https://doi.org/10.1007/s42452-024-06040-8

Subash M, Chandrasekar M, Panimalar S, et al (2022) Pseudo-first kinetics model of copper

doping on the structural, magnetic, and photocatalytic activity of magnesium oxide nanoparticles for energy application. Biomass Convers Biorefinery 13:. https://doi.org/10.1007/s13399-022-02993-1

Taghavi Fardood S, Moradnia F, Heidarzadeh S, Naghipour A (2023) Green synthesis, characterization, photocatalytic and antibacterial activities of copper oxide nanoparticles of copper oxide nanoparticles. Nanochemistry Res 8:134–140. https://doi.org/10.22036/ncr.2023.02.006

Tang W, Pei Y, Zheng H, et al (2022) Twenty years of China's water pollution control: Experiences and challenges. Chemosphere 295:133875. https://doi.org/10.1016/j.chemosphere.2022.133875

Tlili M, Nefzi C, Alhalaili B, et al (2021) Synthesis and Characterization of MgO Thin Films Obtained by Spray Technique for Optoelectronic Applications. Nanomaterials 11:3076. https://doi.org/10.3390/nano11113076

Vasanthi V, Kottaisamy M, Anitha K, Ramakrishnan V (2017) Near UV excitable yellow light emitting Zn doped MgO for WLED application. Superlattices Microstruct 106:174–183. https://doi.org/https://doi.org/10.1016/j.spmi.2017.03.050

Vinayagam R, Singhania B, Murugesan G, et al (2022) Photocatalytic degradation of methylene blue dye using newly synthesized zirconia nanoparticles. Environ Res 214:113785. https://doi.org/https://doi.org/10.1016/j.envres.2022.113785

Wang Y, Gao P, Wei Y, et al (2021) Silver nanoparticles decorated magnetic polymer composites (Fe3O4@PS@Ag) as highly efficient reusable catalyst for the degradation of 4-nitrophenol and organic dyes. J Environ Manage 278:111473. https://doi.org/https://doi.org/10.1016/j.jenvman.2020.111473

Yousefi R, Jamali Sheini F, Cheraghizade M, et al (2015) Enhanced visible-light photocatalytic activity of strontium-doped zinc oxide nanoparticles. Mater Sci Semicond Process 32:152. https://doi.org/10.1016/j.mssp.2015.01.013

Yousefi S, Ghasemi B, Nikolova MP (2021) Opto-structural characterization of Mg(OH)2 and MgO nanostructures synthesized through a template-free sonochemical method. Appl Phys A 127:549. https://doi.org/10.1007/s00339-021-04605-7

Zwijnenburg MA (2021) The effect of particle size on the optical and electronic properties of magnesium oxide nanoparticles. Phys Chem Chem Phys 23:21579–21590. https://doi.org/10.1039/D1CP02683F